Incoherency in Central American hydroclimate proxy records spanning the last millennium

Jonathan Obrist-Farner[1], Byron A. Steinman[2], Nathan D. Stansell[3], and Jeremy Maurer[4]

[1]Missouri S&T
[2]University of Minnesota, Duluth
[3]Northern Illinois University
[4]Missouri University of Science and Technology

November 22, 2022

Abstract

Continued global warming is expected to result in drying of Central America, with projections suggesting a decrease in precipitation. Poor hindcasting of precipitation, however, due in part to spatial and temporal limitations in instrumental data, subjects these projections to considerable uncertainty. Paleoclimate proxy data are therefore critical for understanding regional climate responses during times of global climate reorganization. Here we present two lake-sediment based records of precipitation variability in Guatemala along with a synthesis of Central American hydroclimate records spanning the last millennium (800-2000 CE). The synthesis reveals that regional climate responses have been strikingly heterogeneous, even over relatively short distances. Our analysis further suggests that shifts in the mean position of the Intertropical Convergence Zone, which have been invoked by numerous studies to explain variability in Central American and circum-Caribbean proxy records, cannot alone explain the observed pattern of hydroclimate variability. Instead, interactions between several ocean-atmosphere processes and their disparate influences across variable topography have resulted in complex precipitation responses. These complexities highlight the difficulty of reconstructing past precipitation changes across Central America and point to the need for additional paleo-record development and analysis before the relationships between external forcing and hydroclimate change can be robustly determined. Such efforts should help anchor model-based predictions of future responses to continued global warming.

Incoherency in Central American hydroclimate proxy records spanning the last millennium

Jonathan Obrist-Farner[1], Byron Steinman[2], Nathan Stansell[3], and Jeremy Maurer[1]

[1] Geosciences and Geological and Petroleum Engineering Department, Missouri University of Science and Technology, USA.

[2] Large Lakes Observatory and Department of Earth and Environmental Sciences, University of Minnesota Duluth, USA.

[3] Department of Geology and Environmental Geosciences, Northern Illinois University, USA.

Corresponding author: Jonathan Obrist-Farner (obristj@mst.edu)

Key Points:

- We developed two precipitation proxy records from Central America and compared several hydroclimate records from the region.
- We found that precipitation patterns in Central America are highly heterogenous.
- Disparities among the precipitation records are a result of complex interactions between several ocean-atmosphere processes.

Abstract

Continued global warming is expected to result in drying of Central America, with projections suggesting a decrease in precipitation. Poor hindcasting of precipitation, however, due in part to spatial and temporal limitations in instrumental data, subjects these projections to considerable uncertainty. Paleoclimate proxy data are therefore critical for understanding regional climate responses during times of global climate reorganization. Here we present two lake-sediment based records of precipitation variability in Guatemala along with a synthesis of Central American hydroclimate records spanning the last millennium (800-2000 CE). The synthesis reveals that regional climate responses have been strikingly heterogeneous, even over relatively short distances. Our analysis further suggests that shifts in the mean position of the Intertropical Convergence Zone, which have been invoked by numerous studies to explain variability in Central American and circum-Caribbean proxy records, cannot alone explain the observed pattern of hydroclimate variability. Instead, interactions between several ocean-atmosphere processes and their disparate influences across variable topography have resulted in complex precipitation responses. These complexities highlight the difficulty of reconstructing past precipitation changes across Central America and point to the need for additional paleo-record development and analysis before the relationships between external forcing and hydroclimate change can be robustly determined. Such efforts should help anchor model-based predictions of future responses to continued global warming.

Plain Language Summary

During the last 40 years, Central American precipitation has decreased substantially, creating problems for a region that depends heavily on agriculture. Records suggest, however, that precipitation is not changing uniformly in the region. This differs from climate models that predict uniform drying for the entire Central American region. We set out to investigate Central American climate during the last 1200 years to see if this variability is consistent through time, using precipitation records derived from sediment and speleothems. We acquired two new records from lakes in Guatemala and compare them with existing records from Central America. Our analysis indicates that precipitation has been highly variable across space and time. We suggest that interactions between several atmospheric and oceanic processes produce complex spatiotemporal precipitation variability in the region.

1 Introduction

The last 40 years have been marked by a significant decrease in Central American precipitation (Anderson et al., 2019). Continued global warming will further influence moisture availability in the region (Neelin et al., 2006; Almazroui et al., 2021), potentially through changes in the width, strength and/or position of the Intertropical Convergence Zone (ITCZ; Byrne & Schneider, 2016; Mamalakis et al., 2021). Limitations in regional instrumental data, however, have prevented the robust characterization of precipitation changes in many areas of Central America (CA), and have hindered assessments of climate model hindcasting of precipitation (Imbach et al., 2018). Simulations of future hydroclimate patterns exhibit significant inter-model heterogeneities and fail to replicate the spatially complex precipitation patterns of present day (Christensen et al., 2007; Bhattacharya & Coats, 2020; Fig. 1, Supplementary Figure SF 1), which result from interactions between several ocean-atmosphere processes (Martinez et al., 2019) and steep topographic gradients (Waylen et al., 1996; Imbach et al., 2018). Paleoclimate proxy evidence from Central America is therefore necessary for establishing a long-term perspective on hydroclimate variability that can inform model hindcasting and future projections.

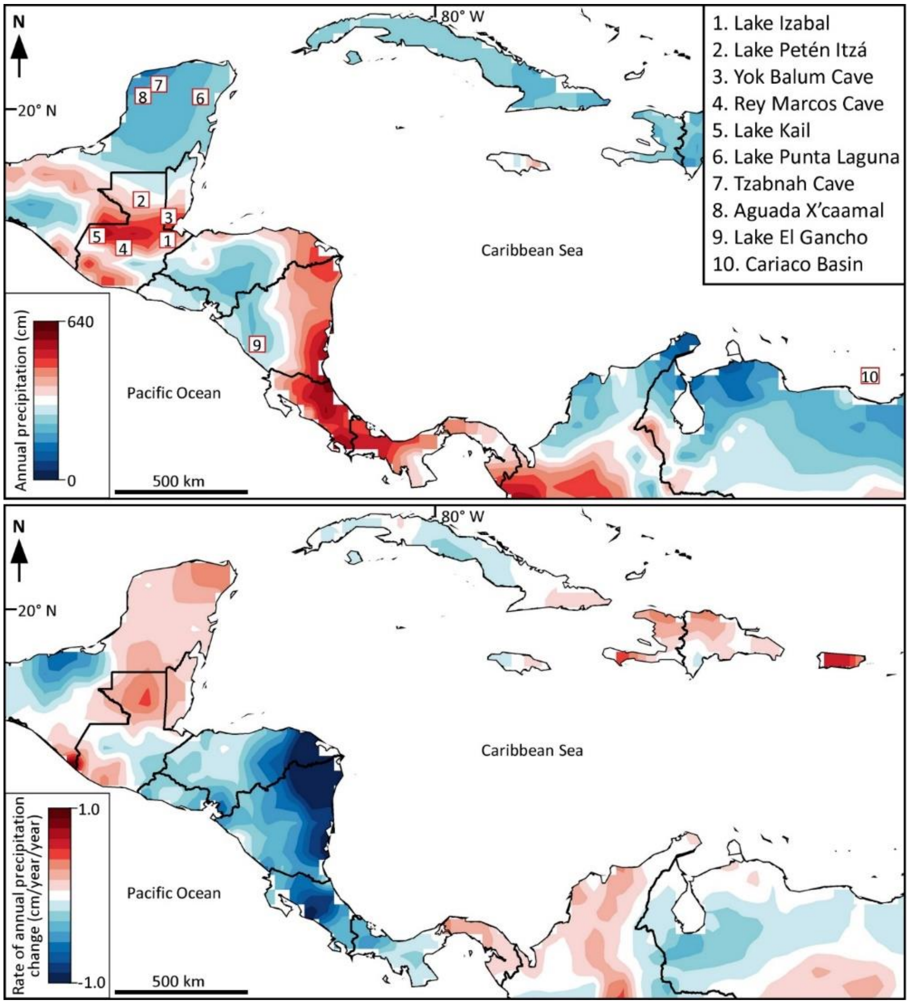

Figure 1. Top: Map of Central America, the Caribbean, and northern South America showing mean annual precipitation based on three gridded data products (Willmott & Matsuura, 2001; Schneider et al., 2011; Harris et al., 2014) spanning the period 1966-2016 CE. Red squares show the location of proxy records mentioned in the text. Bottom: Map showing the mean rate of change in annual precipitation over the same time period with the same data. Note the large gradients in rate of change and mean precipitation in western Central America, especially in the region where large spatial heterogeneity is observed in the proxy records. For both maps, gridded data was interpolated and smoothed.

A substantial body of evidence points to a change in ITCZ dynamics during the last millennium, especially during the Little Ice Age (LIA; ~1300 to 1850 CE), when the ITCZ is hypothesized to have shifted to a more southerly mean position (Haug et al., 2001; Hodell et al., 2005; Bird et al., 2011). Such an occurrence, were it to be conclusively identified in the paleo-proxy data, would provide insight on CA hydroclimate responses to a potential future southward shift in the ITCZ, which some models project should occur as temperatures increase globally (Christensen et al., 2007; Mamalakis et al., 2021). However, proxy evidence from CA is inconsistent, pointing to significant spatial variability in hydroclimate during the LIA. For example, proxy records from the northern Yucatán Peninsula (Hodell et al., 2005) and northern South America (Haug et al., 2001) indicate regional droughts at this time, suggesting a potential southward displacement of the rain belt, while proxy records from Belize (Asmerom et al., 2020), the highland regions of Guatemala (Winter et al., 2020; Stansell et al., 2020), and central Mexico (Lozano-García et al., 2007) do not support this pattern, implying a complex regional hydroclimate response that ITCZ dynamics alone cannot explain. These contrasting results suggest that spatial heterogeneity in precipitation variability could be a persistent feature of CA climate on decadal and longer timescales and that synoptic-scale processes, such as changes in ITCZ mean position, can potentially produce incoherent hydroclimate responses across CA.

Here we present results from radiocarbon-dated sediment cores obtained from two lakes in the Guatemalan lowlands, Lake Petén Itzá (LPI core) and Lake Izabal (LI core). Our results, combined with a synthesis of proxy records from western CA, show evidence of spatially complex patterns of hydroclimate change during the last millennium, especially during the LIA. We assert that the combination of steep topographic gradients and the interaction between several ocean-atmosphere processes is the reason for the heterogenous pattern of hydroclimate variability. Our analysis suggests that the development of additional paleoclimate records is needed to achieve clarity on how precipitation patterns have varied in CA in response to external forcing and synoptic-scale circulation changes.

2 Study Area and Modern Climatology

Modern precipitation in CA is influenced by the North Atlantic Subtropical High (NASH), the ITCZ, the Caribbean Low-Level Jet (CLLJ), and changes in sea-surface temperatures (SSTs) in both the Pacific and Atlantic basins (Martinez et al., 2019; Fig. 2). The interaction of these ocean-atmosphere processes along with large topographic gradients produces complex spatial patterns of precipitation variability in the region (Fig. 1). For example, due to the high topography along the Caribbean coast of CA, the CLLJ promotes orographic uplift, increasing precipitation in the area (Fig. 1). During the summer, easterly winds bifurcate in the western Caribbean Sea, delivering moisture to the Yucatán Peninsula (Wang, 2007). During the winter, easterly winds shift southward away from the Yucatán Peninsula and across the CA Isthmus towards the Pacific Ocean, reducing precipitation in the Yucatán but, through orographic uplift, increasing precipitation in the highland region of Guatemala (Martinez et al., 2019; Duarte et al., 2021). Disparities between the influence of the CLLJ, the ITCZ, and the NASH, combined with topographic complexities, has resulted in different rates of precipitation change across CA during the last 50 years and in differing precipitation amounts at Izabal and Petén Itzá, with the former receiving around twice as much (~3300 mm yr-1 versus ~1800 mm yr-1; Fig. 1).

Lake Petén Itzá is located in northern Guatemala (Fig. 1), having a surface area of 100 km^2, an elevation of ~110 m above mean sea level, and a maximum depth of 160 m. The lake water is dominated by bicarbonate and sulfate, calcium, and magnesium ions (Hodell et al., 2008) with minimal river input. Lake Izabal is in the eastern lowlands of Guatemala at ~1.5 m above mean sea level, with a surface area of 672 km^2 and a maximum depth of 15 m. Lake Izabal contains fresh water (Brinson & Nordlie, 1975), and riverine input is significant due to its large catchment (8740 km^2; Obrist-Farner et al., 2019).

3 Materials and Methods

2.1 Coring

Sediment cores were collected using two piston corers, one for unconsolidated mud-water interface (MWI) sediments (Fisher et al., 1992) and the other, a modified Livingstone corer, for deeper, consolidated sediments (Deevey, 1965). The cores were collected during two field seasons using a wooden platform mounted on two canoes. We collected two sediment cores, one from Lake Petén Itzá (LPI core; 515 cm long) and one from Lake Izabal (LI core; 455 cm long; Fig. 1). In Petén Itzá (16°56′, 89°55′), the MWI core was collected from the side of the platform to a sediment depth of 72 cm in 8.4 m of water. The core was extruded in the field at 2.0-cm intervals, and samples were placed in Whirl-Pak® bags. Next, a PVC casing pipe was lowered through a hole in the center of the platform and forced into the sediment to a depth of 0.5 cm. Once the casing was set and cleaned, six core sections were retrieved, to a depth of 515 cm. In Izabal (15°24’, 89°16’), the MWI core was collected from the side of the platform to a sediment depth of 55 cm in 5.7 m of water. The core was extruded in the field at 3.0-cm intervals, and samples were placed in Whirl-Pak® bags. Next, a PVC casing pipe was lowered through a hole in the center of the platform and forced into the sediment to a depth of 0.5 m. Once the casing was set and cleaned, four core sections were retrieved, to a depth of 455 cm. Sediment cores were kept inside the polycarbonate core barrels and transported to Missouri University of Science and Technology for further analysis.

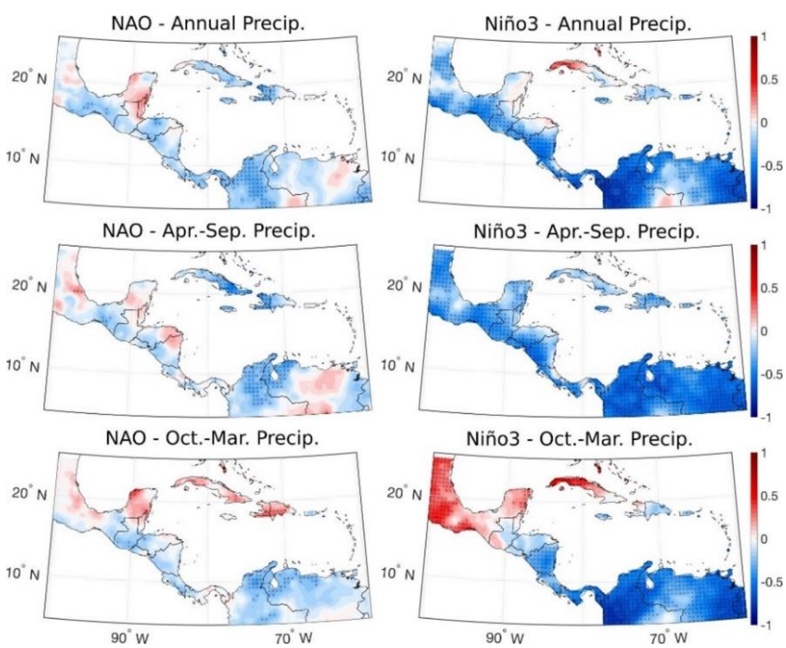

Figure 2. Correlation maps of annual (top), April to September (middle), and October to March (bottom) precipitation amounts and climate indexes including NAO (left) and Niño3 SSTs (right). Precipitation data are based on three ridded data products spanning 1966-2016 CE (Willmott & Matsuura, 2001; Schneider et al., 2011; Harris et al., 2014). Black hatches mark regions of significance ($p < 0.1$). Scale bars depict Pearson’s r values.

2.2 Radiocarbon dating

We obtained accelerator mass spectrometry (AMS) radiocarbon dates from both cores using charcoal and terrestrial wood fragments. Charcoal and wood fragments were washed using deionized water and submitted to the Center for Accelerator Mass Spectrometry at Lawrence Livermore National Laboratory and to the National Ocean Sciences Accelerator Mass Spectrometry (NOSAMS) Facility at Woods Hole Oceanographic Institution. All samples were first treated with a standard acid-base-acid treatment, graphitized, and their radiocarbon concentrations measured via Accelerator Mass Spectrometry. Radiocarbon results were calibrated with OxCal 4.4 (Bronk Ramsey, 2009) using IntCal20 (Reimer et al., 2020). We established age-depth models with the Bayesian software Bacon (Blaauw & Christen, 2011) for the LPI and LI cores (SF2, SF3) using five and seven radiocarbon dates, respectively (ST1, ST2).

2.3 Core scans and photographs

Cores were scanned using a GEOTEK Multi-sensor core logger at the University of Florida and at LacCore facilities at the University of Minnesota. Cores were first scanned for magnetic susceptibility and density and then opened and split in half to obtain line-scan photographs. Sedimentological observations for both cores were carried out on split core surfaces with the aid of the line-scan photographs (Schnurrenberger et al., 2003). Bed color, sedimentary texture and structure, as well as bedding planes were observed and recorded at 1-cm intervals.

The split cores from both locations were analyzed at the Large Lakes Observatory, University of Minnesota, Duluth, USA, using an ITRAX XRF core scanner using a Cr source tube at 30 kV and 55 mA at 5-mm resolution with a 15-second dwell time (SF4, SF5). Raw data were reprocessed to optimize peak-fitting, using QSpec 8.6.0 software (ST3, ST4). In addition, X-radiographs were collected using a Cr source tube run at 60 kV and 30 mA, with variable exposure times, depending on the sediment density. We performed principal component analysis (PCA) in ©MATLAB to investigate the relationship between elements, which allows to represent a multivariate data set as a smaller set of variables to interpret trends or changes in the sediment cores through time. Before PCA analysis, all elemental counts were standardized (converted to z-scores) to avoid confounding effects of dimensional heterogeneity. We utilized the combination of elemental abundances, elemental ratios, and PCA analysis to infer changes in lake catchment and in-lake processes. Elemental ratios discussed in the text are presented on a logarithmic scale due to the asymmetry associated with ratios. Finally, we did not carry out XRF analyses on the upper 50 cm of both cores due to the confounding effects of high water content on XRF analysis (MacLachlan et al., 2015).

2.4 Proxy data age-depth modeling and uncertainty analysis

We assembled eleven hydroclimate proxy records from lake sediment cores, marine sediment cores, and speleothems, and focused our analysis on 800 to 2000 CE. All proxy records were obtained from the NOAA/World Data Service for Paleoclimatology archives website (https://www.ncei.noaa.gov/access/paleo-search/). For all proxy records, we obtained the published radiocarbon (sediment cores) and U-Th (speleothems) dates and their uncertainties and utilized Bacon (Blaauw & Christen, 2011) to generate age-depth relationships (SF 2, 3, 8-16). For all proxy sites, an additional date was introduced to constrain the most recent year of the record (i.e., the year of sample collection). For the radiocarbon-based age-depth models, we used IntCal20 (Reimer et al., 2020) to calibrate the dates. For the Cariaco Basin marine record, we used the published calibrated ages because the radiocarbon ages and the associated uncertainties were not available. For U-Th speleothem models, we used the calibrated U-Th ages and their uncertainties.

Bacon (compiled in R) uses the radiocarbon dates and the other age-control points (e.g., date of core collection or U-Th dates) to model sedimentation rates for sediment cores and growth rates for speleothems and provides age uncertainty quantification.

For the uncertainty analysis, 1000 age-depth pairs were obtained from Bacon, allowing us to generate 1000 age-proxy pairs for each record. We utilized the 1000 age-proxy pairs and resampled them at 5-year intervals using a linear interpolation. We used ©MATLAB to assemble age-model iterations for each proxy site, resulting in a range of proxy values for a specific modeled age (SF 17-27). We used the 1000 age-proxy pairs and calculated correlation coefficients and significance (p-values) and report the mean and 1σ for correlation values and the mean p-value. We used Bretherton's et al. (1999) formula for the effective sample size (ESS) given two time series X and Y (their equation 30):

$$ESS = N \frac{1}{\sum_{i=-(N-1)}^{(N-1)} \left(1 - \frac{|i|}{N}\right) \rho_i^X \rho_i^Y}$$

where N is the number of matching samples in both series, and the ρi's are the ith-lag autocorrelation coefficients of the individual time series. This is the more general expression of their equation 31:

$$ESS = N \frac{1 - \rho_1^X \rho_1^Y}{1 + \rho_1^X \rho_1^Y}$$

which is only valid when $\boldsymbol{\rho_1^X}, \boldsymbol{\rho_1^Y} \ll 1$.

3 Results and Interpretations

For both studied cores, the ages of the terrestrial wood fragments are in stratigraphic order. The 515 cm-long LPI core covers the last ~7000 years (Obrist-Farner & Rice, 2019; SF 2, ST 1), while the 455 cm-long LI core is much shorter, covering the last ~1400 years (Hernández et al., 2020; SF 3, ST 2). Our results utilize the weighted mean modeled ages for both cores and are focused on the uppermost 50 to 115 cm (800 to 1585 CE) from the LPI core and on the segment between 55 and 435 cm (800 to 1926 CE) from the LI core.

The 65-cm-long segment of the LPI core is characterized by thinly bedded carbonaceous mud that alternates in color between dark and light gray (Obrist-Farner & Rice, 2019). The mud contains variable amounts of gastropod shells and scattered organic debris. PCA analysis of elemental abundances shows that PC1 predominantly captures variability in terrigenous elements derived from bedrock erosion (Ti, Al, Fe, K, and Si). The first principal component (PC1) explains 62.2% of the variance in the LPI data (Fig. 3), and we infer that changes in the PC1 score through time indicate changes in catchment erosion and runoff (e.g., Kylander et al., 2011; Davies et al., 2015; Duarte et al., 2021). The second principal component (PC2) explains variations related mostly to Sr and Ca (Fig. 3) and explains an additional 19.0% of the total variance. We infer that changes in PC2 scores reflect the presence of evaporites, potentially during times of low lake levels, reduced precipitation, and/or increased evaporation (e.g., Mueller et al., 2009; Kylander et al., 2011; Davies et al., 2015; Fig. 3). Similarly, we utilize the ratio of Ca over Ti as a proxy for increased evaporation (e.g., Mueller et al., 2009; Kylander et al., 2011; Davies et al., 2015), in support of our PC2 results.

From ~800 to ~1200 CE, elemental abundances from terrigenous elements (e.g., Ti, Al, and Si) decrease along with PC1 (SF 4, ST 3), indicating reduced catchment erosion for Lake Petén Itzá (Fig. 3). During this time, there is a slight increase in Ca and S, in PC2 scores, and in the log(Ca/Ti) ratio. After ~1200 CE, Ti, Al, Si, and K decrease and PC1 scores decline rapidly, while PC2 scores and the log(Ca/Ti) ratio exhibit a pronounced increase. These results suggest an increase in evaporation at Lake Petén Itzá that peaked at ~1320 CE. After ~1320 CE, terrigenous elemental abundance and PC1 scores remain low, and both PC2 scores and the log(Ca/Ti) ratio decrease toward the uppermost part of the interval, indicating continued low catchment erosion and a decrease in evaporation.

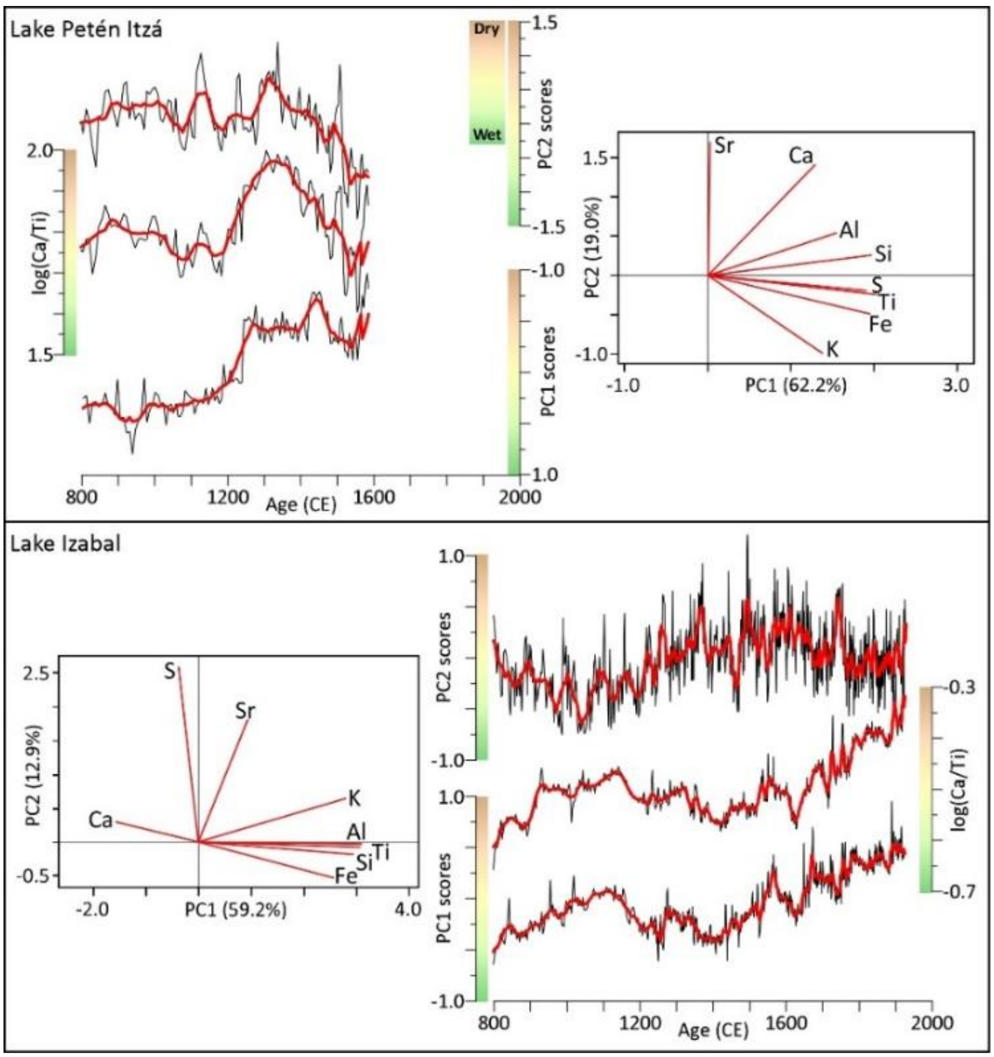

Figure 3. Principal component analysis for selected elemental abundances and time series data (black lines) and 10-point running mean (red lines) showing PC1 scores, log(Ca/Ti), and PC2 scores from lakes Petén Itzá and Izabal. See SF 4 and SF 5 for additional results.

The 400-cm-long segment of the LI core is characterized by homogeneous olive gray silty mud that is faintly laminated and very thinly bedded with minimal organic debris (Hernández et al., 2020). The PCA results show that PC1, which explains 59.2% of the variance, mainly captures variability in Ti, Al, Si, Fe, and K (Fig. 3). We infer that positive PC1 scores indicate an increase in catchment erosion and runoff (e.g., Kylander et al., 2011; Davies et al., 2015; Duarte et al., 2021; Fig. 3). PC2 for the LI core is mostly related to changes in Sr and S and explains 12.9% of the total variance. The processes that PC2 reflect at Lake Izabal are ambiguous because S and Sr in the lake can be related to evaporation, marine water transgression, or redox processes (Duarte et al., 2021; Obrist-Farner et al., 2022).

From ~800 to ~1140 CE, there is a decrease in both PC1 and terrigenous elemental abundances, such as Ti, Al, K, and Si (Fig. 3, SF 5, ST 4). Similarly, there is an increase in the log(Ca/Ti) ratio and a decrease in PC2 scores. From ~1140 to ~1410 CE, there is an increase in PC1 scores and a decrease in the log(Ca/Ti) ratio, while PC2 scores are variable but generally increase. These results suggest a decrease in catchment erosion and runoff in the Lake Izabal area from ~800 to 1140 CE, followed by an increase from 1140 to 1410 CE. After ~1410 CE, PC1 scores decrease and the log(Ca/Ti) ratio increases, supporting a decrease in catchment erosion and runoff. PC2 scores are highly variable after ~1410 CE.

4 Discussion

There are at least two processes that could potentially explain the spatiotemporal variability in the proxy data from Petén Itzá and Izabal. First, changes in catchment erosion could have resulted from agricultural practices and deforestation in the catchments of both lakes. Paleolimnological investigations in Guatemala and the Yucatán Peninsula have shown that there was a significant increase in catchment erosion during times of increased agricultural activities in the area, especially during the apogee of the Maya civilization (Brenner et al., 2002). Human settlements in the region were at their maximum extent at ~800 CE, resulting in significant erosion, as observed in sediment cores from many Petén lakes (Brenner et al., 2002). The collapse and disintegration of large cities led to rapid forest recovery (Curtis et al., 1998) with a coeval decrease in catchment erosion after ~1000 CE. Our Lake Petén Itza record indicates a decrease in erosion in the area starting at ~1200 CE with a minimum in catchment erosion at ~1350 CE (95% range 1230-1420), while the Izabal record indicates an increase in erosion at ~1140 CE with a maximum occurring at ~1410 CE (95% range 1300-1440). Although deforestation and agricultural practices undoubtedly had some influence, it is unlikely that the observed differences in the two records are solely due to these processes.

A second possible mechanism for explaining the differences in the Petén Itzá and Izabal records is that the inferred changes in catchment erosion, as well as changes in evaporation, resulted from different hydroclimate patterns at the two locations. For example, the decrease in erosion and increase in evaporation from 800 to ~1100 CE in both records could reflect a decrease in precipitation and increase in evaporation during the well-known Maya droughts (Hodell et al., 1995; Kennett et al., 2012). Between 800 to 1100 CE the two lake records are similar to other paleoclimate datasets from Guatemala, Belize, and the Yucatán Peninsula that suggest a decrease in precipitation at that time (e.g., Douglas et al., 2016). However, after this interval, the records diverge, with the Petén data indicating a decrease in erosion at ~1350 CE and the Izabal record showing a maximum in erosion at ~1410 CE that is highly unlikely to have resulted from human disturbance given the known decline in major Mayan population centers well before this time. This difference instead suggests spatially complex and inconsistent hydroclimate in western CA, especially after 1100 CE.

Comparison of paleoclimate records from CA reveals that, much like with Izabal and Petén Itzá, inconsistency between records is the norm, even over relatively short distances and especially during the LIA (Figs. 4, 5). Notably, assessment of the relationship between proxy records is made difficult by the uncertainties in radiocarbon and U-Th age-depth models and by the inherent differences in each of the proxy systems. For example, lakes of different sizes and degrees of hydrological closure should be expected to respond differently to changes in hydroclimate, and lake sediment archives from closed-basin settings will not capture the same information as speleothem isotope records, with the former reflecting the balance between evaporation and precipitation and the latter typically reflecting precipitation amount (Hodell et al., 1995; Lachniet, 2009). However, the substantial disparities between the proxy records exist even when comparing only speleothem records (SF 6), when comparing records from similar lacustrine systems (SF 7), and when considering age-depth model uncertainties (Figs. 4, 5). For example, the YOK-G speleothem $\delta^{13}C$ record from Belize (Asmerom et al., 2020; ~70 km north from Izabal) is negatively correlated with Izabal ($r = -0.44 \pm 0.08$; Fig. 5) and indicates wetter than average conditions from ~1400 to ~1850 CE, while both Izabal and the YOK-I speleothem $\delta^{18}O$ record (Kennett et al., 2012) are positively correlated ($r = 0.30 \pm 0.06$) and indicate peak precipitation at 1300-1410 CE and dryer conditions thereafter (Fig. 4). The Yok Balum records themselves exhibit a weak negative correlation ($r = -0.20 \pm 0.05$; Fig. 5), indicating that these two speleothem records from the same cave are not consistent. Additionally, the $\delta^{18}O$ record from Lake Kail in the western highlands (Stansell et al., 2020; ~250 km west from Izabal) and the Rey Marcos speleothem in the central highlands of Guatemala (Winter et al., 2020; ~100 km west from Izabal) do not exhibit significant correlations with Izabal or Petén Itzá (Figs. 4, 5) and indicate minimal change in precipitation and a reduction in precipitation at ~1350 CE, respectively. The $\delta^{18}O$ record from Lake Punta Laguna (Curtis et al., 1996) is negatively correlated with Izabal ($r = -0.29 \pm 0.10$) and Petén Itzá ($r = 0.20 \pm 0.14$; Figs. 4, 5) and indicates less precipitation between ~1150 and ~1400 CE and wetter conditions thereafter. In contrast, the Aguada X'caamal $\delta^{18}O$ record (Hodell et al., 2005; ~240 km west from Lake Punta Laguna) is positively correlated with Izabal ($r = 0.50 \pm 0.10$) and Petén Itzá ($r = 0.52 \pm 0.16$; Figs. 4, 5) and indicates persistently dry conditions after ~1250 CE. The Tzabnah Cave Chaac $\delta^{18}O$ record from the Yucatán Peninsula (Medina-Elizalde et al., 2010; ~40 km northeast from Aguada X'caamal) is negatively correlated with Izabal ($r = -0.20 \pm 0.09$) and Petén Itzá ($r = -0.13 \pm 0.13$) and indicates alternating dry and wet periods during the LIA.

Comparison between more distant records also supports our inference of profound hydroclimate heterogeneity in CA. The $\delta^{18}O$ record from Lake El Gancho in Nicaragua (Stansell et al., 2013) is positively correlated with Izabal ($r = 0.44 \pm 0.12$; Fig. 5) and weakly correlated with Petén Itzá ($r = 0.30 \pm 0.18$; Fig. 5) and indicates one short wet period between ~1400-1550 CE within an overall drying trend (Figs. 4, 5), similar to the observations from the Izabal and the YOK-I speleothem records. The onset of drying inferred from the Izabal record and the Cariaco Basin Ti record (Haug et al., 2001) are similar ($r = 0.33 \pm 0.14$; Fig. 5); however, Petén Itzá indicates a reduction in precipitation at ~1350 CE, ~400 years earlier than the driest time in northern Venezuela (Fig. 4). Out of the 11 proxy records analyzed, only two of 55 cross-correlations are statistically significant ($p < 0.1$; Figs. 4, 5; see Supplementary Material), highlighting the significant inconsistencies in regional hydroclimate proxy records.

It is difficult to reconcile the distinct differences in hydroclimate proxy records from CA by invoking changes in ITCZ dynamics alone. A southward shift in the ITCZ during the LIA (Haug et al., 2001; Hodell et al., 2005) would have produced persistent regional droughts during boreal summer if changes in the mean zonal position of the ITCZ were the only factor. Our analysis does not support this inference, indicating that other ocean-atmosphere processes as well as local climate controls related to complex topography must be responsible for the complex, regionally heterogeneous hydroclimate changes observed in the CA proxy records.

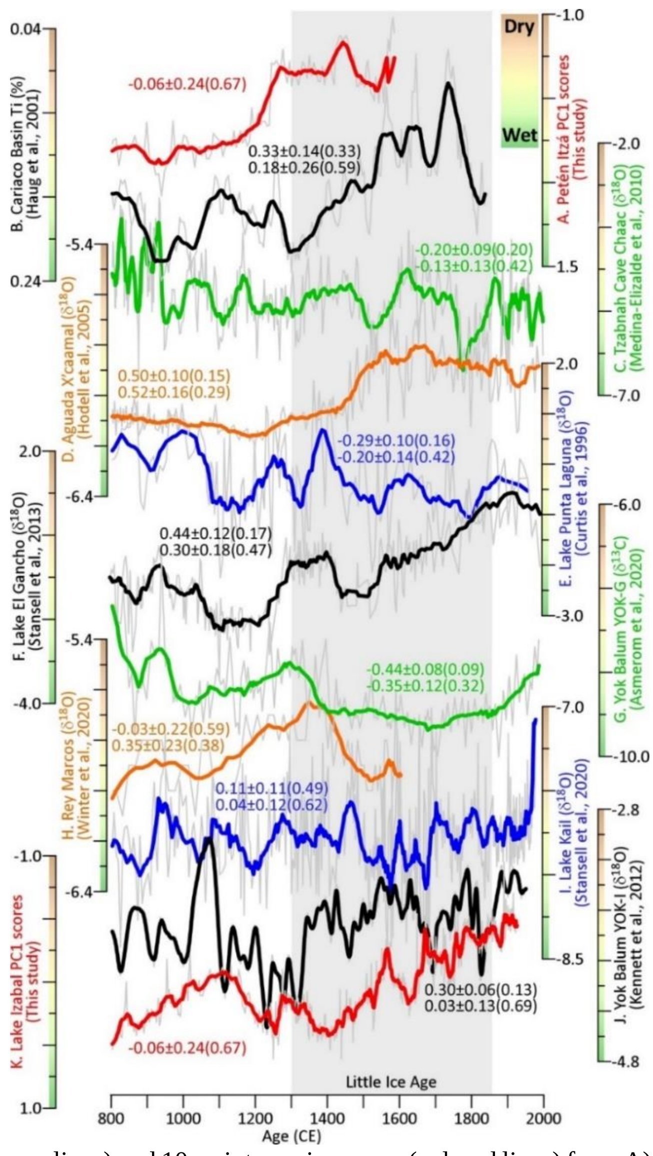

Figure 4. Proxy time series (gray lines) and 10-point running mean (colored lines) from A) Lake Petén Itzá, B) Cariaco Basin, C) Chaac speleothem, D) Aguada X'caamal, E) Lake Punta Laguna, F) Lake El Gancho, G) Yok Balum YOK-G, H) Rey Marcos, I) Lake Kail, J) Yok Balum YOK-I, and K) Lake Izabal. Numbers show mean correlation coefficient values, 1σ, and p-values (see Figure 5) for the time series versus Izabal (upper numbers) and Petén Itzá (lower numbers).

Asmerom et al. (2020) hypothesized that during the LIA, the ITCZ became wider and weaker, resulting in a decrease in precipitation in northern Venezuela and in an increase along the northern flanks of the rain belt. However, the drying trend after the onset of the LIA inferred from Izabal and the YOK-I speleothem (Fig. 4) does not support this hypothesis. That the ITCZ became wider/weaker during the LIA also fails to explain how the Petén region could have become drier at this time, as suggested by the proxy data from Lake Petén Itzá and from Aguada X'caamal. An alternative hypothesis is that moisture availability in western CA was affected by SST gradients between the Pacific and Atlantic oceans (Metcalfe et al., 2015; Bhattacharya & Coats, 2020) through changes in the El Niño Southern Oscillation (ENSO) and the North Atlantic Oscillation (NAO). Modern precipitation analysis indicates that positive ENSO events result in reduced precipitation across the entire Pacific coast of Central America (Dai & Wigley, 2000), whereas positive NAO conditions result in an increase in precipitation along the eastern coast of Guatemala, Belize, and the Yucatán Peninsula (Stansell et al., 2020; Fig. 2). During the beginning of the last millennium, La Niña-like conditions (Cobb et al., 2003) and a more positive NAO (Mann et al., 2009) would have produced a wetter climate in both the Pacific coast of Central America and on the eastern coast of Guatemala, Belize, and the Yucatán Peninsula. In contrast, during the LIA, a change to El Niño-like conditions and a more negative NAO (Cobb et al., 2003; Mann et al., 2009)

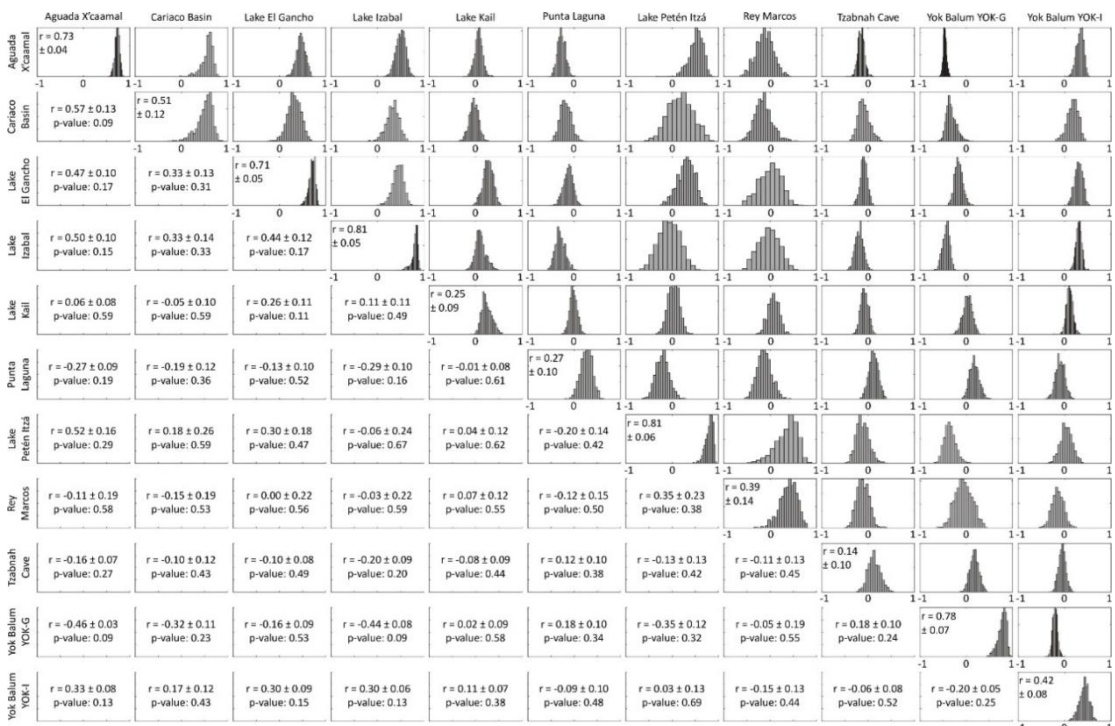

would have resulted in a drier climate across almost all of CA. Our proxy record synthesis indicates a regionally incoherent pattern of hydroclimate change during the last millennium, and especially during the LIA, that likely was not predominantly controlled by any one of these processes, and instead suggests that a combination of factors controls hydroclimate patterns in CA on multidecadal and longer timescales.

Figure 5. Matrix showing the range of correlation values (upper right) for all proxy record realizations utilizing 1000 age-proxy pairs (see supplementary information). The diagonal quantifies the uncertainties in the age-depth model; for example, an age-depth model with no uncertainty would have correlation equal to 1. Each distribution represents how correlated each pair of sets of 1000 age-proxy realizations are to each other (see Supplementary

Material). The lower left shows mean correlation values, ±1σ, and mean p-values for the records analyzed. The $\delta^{18}O$ records been multiplied by negative one so that positive correlation indicates consistent behavior between proxy sites.

One potential mechanism that could further explain the CA proxy record patterns is a change in the intensity of the CLLJ along with topographic controls on moisture delivery to the region. Expansion of the western edge of the NASH could have resulted in a diversion of the CLLJ, the main source of moisture to western CA (Hastenrath, 1984). A southward shift in the CLLJ, combined with steep topography along the Caribbean coast, would have the potential to produce an increase in precipitation at Izabal through enhanced convergence via orographic uplift along with a reduction in precipitation at Petén Itzá. Alternatively, changes in Caribbean SSTs and the Atlantic Warm Pool could have resulted in an increase in moisture availability (Winter et al., 2020; Duarte et al., 2021) and through orographic uplift, increase precipitation along the Caribbean coast and central highlands of Guatemala. Both mechanisms, however, still do not explain why records in the Yucatán Peninsula and other regions of Guatemala show disparate hydroclimate signals over the last millennium and in particular the LIA (Figs. 4, 5).

5 Conclusions

Our results highlight that interactions between numerous ocean-atmosphere processes, including the CLLJ, NAO, ENSO, and changes in ITCZ dynamics, as well as the effects of topography, make it difficult to understand external forcing impacts on hydroclimate in CA. Modern-day precipitation patterns are also spatially complex, with large differences in precipitation amounts over short distances, especially along the mountain ranges and coasts of CA. The available hydroclimate proxy data do not support a simple explanation for hydroclimate variability during the last millennium, in particular that ITCZ dynamics (i.e., changes in latitudinal mean position, width and/or strength) were the main driver of hydroclimate change in the absence of other major controlling factors. Instead, the proxy data suggest that several processes must have interacted to produce the inferred precipitation patterns across the northern tropical rainbelt. Additional proxy records from previously unexplored regions, such as the highland region and Pacific and Caribbean coasts of CA could help clarify and disentangle the influence of the various ocean-atmosphere circulation mechanisms on CA hydroclimate.

Acknowledgments

We thank Oscar Nuñez, Heidy Garcia, Elmer Tun Pana, Noe Hernandez, and Defensores de la Naturaleza who provided lake access and helped us collect the sediment cores. We thank Anders Noren and Kristina Brady Shannon from the National Lacustrine Core Facility (LacCore) for help with core analyses and Robert Brown at the University of Minnesota-Duluth for help with XRF scanning. This is contribution #12 of the MCTF research group. The authors have no known conflicts of interest.

Data Availability

Data for replicating the results of this study are available as supplementary files. Additional paleoclimate proxy datasets are available at the National Oceanic and Atmospheric

Administration National Centers for Environmental Information paleoclimate data repository (https://www.ncei.noaa.gov/products/paleoclimatology).

References

Almazroui, M., Islam, M. N., Saeed, F., Saeed, S., Ismail, M., Ehsan, M. A., et al. (2021). Projected changes in temperature and precipitation over the United States, Central America, and the Caribbean in CMIP6 GCMs. *Earth Systems and Environment, 5*(1), 1-24. https://doi.org/10.1007/s41748-021-00199-5

Anderson, T. G., Anchukaitis, K. J., Pons, D., & Taylor, M. (2019). Multiscale trends and precipitation extremes in the Central American Midsummer Drought. *Environmental Research Letters, 14*(12), 124016. http://dx.doi.org/10.1088/1748-9326/ab5023

Asmerom, Y., Baldini, J. U. L., Prufer, K. M., Polyak, V. J., Ridley, H. E., Aquino, V. V., et al. (2020). Intertropical convergence zone variability in the Neotropics during the Common Era. *Science Advances, 6*(7), eaax3644. https://doi.org/10.1126/sciadv.aax3644

Bhattacharya, T., & Coats, S. (2020). Atlantic-Pacific gradients drive last millennium hydroclimate variability in Mesoamerica. *Geophysical Research Letters, 47*(13), e2020GL088061. https://doi.org/10.1029/2020GL088061.

Bird, B. W., Abbott, M. B., Vuille, M., Rodbell, D. T., Stansell, N. D., & Rosenmeier, M. F. (2011). A 2,300-year-long annually resolved record of the South American summer monsoon from the Peruvian Andes. *Proceedings of the National Academy of Sciences, 108*(21), 8583. https://doi.org/10.1073/pnas.1003719108

Blaauw, M., & Christen, J. A. (2011). Flexible paleoclimate age-depth models using an autoregressive gamma process. *Bayesian Anal., 6*(3), 457-474. https://projecteuclid.org:443/euclid.ba/1339616472

Brenner, M., Rosenmeier, M. F., Hodell, D. A., & Curtis, J. H. (2002). Paleolimnology of the Maya lowlands: long-term perspectives on interactions among climate, environment, and humans. *Ancient Mesoamerica, 13*, 141-157. https://www.jstor.org/stable/26308050

Bretherton, C. S., Widmann, M., Dimnikov, V. P., Wallace, J. M., & Blade, I. (1999). The effective number of spatial degrees of freedom of a time-varying field. *Journal of Climate, 12*(7), 1990-2009. https://doi.org/10.1175/1520-0442(1999)012<1990:TENOSD>2.0.CO;2

Brinson, M. M., & Nordlie, F. G. (1975). II. Lakes. 8. Central and South America: Lake Izabal, Guatemala. *SIL Proceedings, 1922-2010, 19*(2), 1468-1479. https://doi.org/10.1080/03680770.1974.11896206

Bronk Ramsey, C. (2009). Bayesian analysis of radiocarbon dates. *Radiocarbon, 51*, 337-360.

Byrne, M. P., & Schneider, T. (2016). Narrowing of the ITCZ in a warming climate: Physical mechanisms. *Geophysical Research Letters, 43*(21), 11,350-311,357. https://doi.org/10.1002/2016GL070396

Christensen, J. H., Hewitson, B., Busuioc, A., Chen, A., Gao, X., Held, I., et al. (Eds.). (2007). *Regional climate projections*. Cambridge: Cambridge University Press.

Cobb, K. M., Charles, C. D., Cheng, H., & Edwards, R. L. (2003). El Niño/Southern Oscillation and tropical Pacific climate during the last millennium. *Nature, 424*(6946), 271-276. https://doi.org/10.1038/nature01779

Curtis, J. H., Brenner, M., Hodell, D. A., Balser, R. A., Islebe, G. A., & Hooghiemstra, H. (1998). A multi-proxy study of Holocene environmental change in the Maya Lowlands of

Peten, Guatemala. *Journal of Paleolimnology, 19*(2), 139-159. https://doi.org/10.1023/A:1007968508262
Curtis, J. H., Hodell, D. A., & Brenner, M. (1996). Climate variability on the Yucatan Peninsula (Mexico) during he past 3500 years, and implications for Maya cultural evolution. *Quaternary Research, 46*(1), 37-47. https://doi.org/10.1006/qres.1996.0042
Dai, A., & Wigley, T. M. L. (2000). Global patterns of ENSO-induced precipitation. *Geophysical Research Letters, 27*(9), 1283-1286. https://doi.org/10.1029/1999GL011140
Davies, S. J., Lamb, H. F., & Roberts, S. J. (2015). Micro-XRF Core Scanning in Palaeolimnology: Recent Developments. In I. W. Croudace & R. G. Rothwell (Eds.), *Micro-XRF Studies of Sediment Cores: Applications of a non-destructive tool for the environmental sciences* (pp. 189-226). Dordrecht: Springer Netherlands.
Deevey, E. S. (1965). Sampling lake sediments by use of the Livingstone sampler. In B. Kummel & D. Raup (Eds.), *Handbook of paleontological techniques* (pp. 521-529). San Francisco: Freeman.
Douglas, P. M. J., Demarest, A. A., Brenner, M., & Canuto, M. A. (2016). Impacts of climate change and the collapse of lowland Maya civilization. *Annual Review of Earth and Planetary Sciences, 44*(1), 613-645. https://doi.org/10.1146/annurev-earth-060115-012512
Duarte, E., Obrist-Farner, J., Correa-Metrio, A., & Steinman, B. A. (2021). A progressively wetter early through middle Holocene climate in the eastern lowlands of Guatemala. *Earth and Planetary Science Letters, 561*, 116807. https://doi.org/10.1016/j.epsl.2021.116807
Fisher, M. M., Brenner, M., & Reddy, K. R. (1992). A simple, inexpensive piston corer for collecting undisturbed sediment/water interface profiles. *Journal of Paleolimnology, 7*(2), 157-161. https://doi.org/10.1007/BF00196870
Harris, I., Jones, P. D., Osborn, T. J., & Lister, D. H. (2014). Updated high-resolution grids of monthly climatic observations – the CRU TS3.10 Dataset. *International Journal of Climatology, 34*(3), 623-642. https://doi.org/10.1002/joc.3711
Hastenrath, S. (1984). Interannual variability and annual cycle: Mechanisms of circulation and climate in the tropical Atlantic sector. *Monthly Weather Review*, *112*, 1097-1107. https://doi.org/10.1175/1520-0493(1984)112%3C1097:IVAACM%3E2.0.CO;2
Haug, G. H., Hughen, K. A., Sigman, D. M., Peterson, L. C., & Röhl, U. (2001). Southward migration of the Intertropical Convergence Zone through the Holocene. *Science, 293*(5533), 1304. https://doi.org/10.1126/science.1059725
Hernández, E., Obrist-Farner, J., Brenner, M., Kenney, W. F., Curtis, J. H., & Duarte, E. (2020). Natural and anthropogenic sources of lead, zinc, and nickel in sediments of Lake Izabal, Guatemala. *Journal of Environmental Sciences, 96*, 117-126. https://doi.org/10.1016/j.jes.2020.04.020
Hodell, D. A., Anselmetti, F. S., Ariztegui, D., Brenner, M., Curtis, J. H., Gilli, A., et al. (2008). An 85-ka record of climate change in lowland Central America. *Quaternary Science Reviews, 27*(11–12), 1152-1165. https://doi.org/10.1016/j.quascirev.2008.02.008
Hodell, D. A., Brenner, M., Curtis, J. H., Medina-González, R., Ildefonso-Chan Can, E., Albornaz-Pat, A., & Guilderson, T. P. (2005). Climate change on the Yucatan Peninsula during the Little Ice Age. *Quaternary Research, 63*(2), 109-121. https://doi.org/10.1016/j.yqres.2004.11.004

Hodell, D. A., Curtis, J. H., & Brenner, M. (1995). Possible role of climate in the collapse of Classic Maya civilization. *Nature*, *375*, 391-394. https://doi.org/10.1038/375391a0

Imbach, P., Chou, S. C., Lyra, A., Rodrigues, D., Rodriguez, D., Latinovic, D., et al. (2018). Future climate change scenarios in Central America at high spatial resolution. PLOS ONE, 13(4), e0193570. https://doi.org/10.1371/journal.pone.0193570

Kennett, D. J., Breitenbach, S. F. M., Aquino, V. V., Asmerom, Y., Awe, J., Baldini, J. U. L., et al. (2012). Development and disintegration of Maya political systems in response to climate change. *Science*, *338*(6108), 788-791. https://doi.org/10.1126/science.1226299

Kylander, M. E., Ampel, L., Wohlfarth, B., & Veres, D. (2011). High-resolution X-ray fluorescence core scanning analysis of Les Echets (France) sedimentary sequence: new insights from chemical proxies. *Journal of Quaternary Science*, *26*(1), 109-117. https://doi.org/10.1002/jqs.1438

Lachniet, M. S. (2009). Climatic and environmental controls on speleothem oxygen-isotope values. Quaternary Science Reviews, 28(5), 412-432. https://doi.org/10.1016/j.quascirev.2008.10.021

Lozano-García, M. d. S., Caballero, M., Ortega, B., Rodríguez, A., & Sosa, S. (2007). Tracing the effects of the Little Ice Age in the tropical lowlands of eastern Mesoamerica. *Proceedings of the National Academy of Sciences*, *104*(41), 16200. https://doi.org/10.1073/pnas.0707896104

MacLachlan, S. E., Hunt, J. E., & Croudace, I. W. (2015). An Empirical Assessment of Variable Water Content and Grain-Size on X-Ray Fluorescence Core-Scanning Measurements of Deep Sea Sediments. In I. W. Croudace & R. G. Rothwell (Eds.), *Micro-XRF Studies of Sediment Cores: Applications of a non-destructive tool for the environmental sciences* (pp. 173-185). Dordrecht: Springer Netherlands.

Mamalakis, A., Randerson, J. T., Yu, J.-Y., Pritchard, M. S., Magnusdottir, G., Smyth, P., et al. (2021). Zonally contrasting shifts of the tropical rain belt in response to climate change. *Nature Climate Change*, *11*(2), 143-151. https://doi.org/10.1038/s41558-020-00963-x

Mann M., E., Zhang, Z., Rutherford, S., Bradley Raymond, S., Hughes Malcolm, K., Shindell, D., et al. (2009). Global signatures and dynamical origins of the Little Ice Age and Medieval Climate Anomaly. *Science*, *326*(5957), 1256-1260. https://doi.org/10.1126/science.1177303

Martinez, C., Goddard, L., Kushnir, Y., & Ting, M. (2019). Seasonal climatology and dynamical mechanisms of rainfall in the Caribbean. *Climate Dynamics*, *53*(1), 825-846. https://doi.org/10.1007/s00382-019-04616-4

Medina-Elizalde, M., Burns, S. J., Lea, D. W., Asmerom, Y., von Gunten, L., Polyak, V., et al. (2010). High resolution stalagmite climate record from the Yucatán Peninsula spanning the Maya terminal classic period. *Earth and Planetary Science Letters*, *298*(1), 255-262. https://doi.org/10.1016/j.epsl.2010.08.016

Metcalfe, S. E., Barron, J. A., & Davies, S. J. (2015). The Holocene history of the North American Monsoon: 'known knowns' and 'known unknowns' in understanding its spatial and temporal complexity. *Quaternary Science Reviews*, *120*, 1-27. https://doi.org/10.1016/j.quascirev.2015.04.004

Mueller, A. D., Islebe, G. A., Hillesheim, M. B., Grzesik, D. A., Anselmetti, F. S., Ariztegui, D., et al. (2009). Climate drying and associated forest decline in the lowlands of northern Guatemala during the late Holocene. *Quaternary Research*, *71*(2), 133-141. https://doi:10.1016/j.yqres.2008.10.002

Neelin, J. D., Münnich, M., Su, H., Meyerson, J. E., & Holloway, C. E. (2006). Tropical drying trends in global warming models and observations. *Proceedings of the National Academy of Sciences*, *103*(16), 6110-6115. https://doi.org/10.1073/pnas.0601798103

Obrist-Farner, J., Brenner, M., Curtis, J. H., Kenney, W. F., & Salvinelli, C. (2019). Recent onset of eutrophication in Lake Izabal, the largest water body in Guatemala. *Journal of Paleolimnology*, *62*(4), 359-372. https://doi.org/10.1007/s10933-019-00091-3

Obrist-Farner, J., Brenner, M., Stone, J. R., Wojewódka-Przybył, M., Bauersachs, T., Eckert, A., et al. (2022). New estimates of the magnitude of the sea-level jump during the 8.2 ka event. *Geology*, *50*(1), 86-90. https://doi.org/10.1130/G49296.1

Obrist-Farner, J., & Rice, P. M. (2019). Nixtun-Ch'ich' and its environmental impact: Sedimentological and archaeological correlates in a core from Lake Petén Itzá in the southern Maya lowlands, Guatemala. *Journal of Archaeological Science: Reports*, *26*, 101868. https://doi.org/10.1016/j.jasrep.2019.05.033

Reimer, P. J., Austin, W. E. N., Bard, E., Bayliss, A., Blackwell, P. G., Bronk Ramsey, C., et al. (2020). The IntCal20 Northern Hemisphere radiocarbon age calibration curve (0–55 cal kBP). *Radiocarbon*, *62*(4), 725-757. https://doi.org/10.1017/RDC.2020.41

Sachs, J. P., Sachse, D., Smittenberg, R. H., Zhang, Z., Battisti, D. S., & Golubic, S. (2009). Southward movement of the Pacific intertropical convergence zone AD 1400–1850. *Nature Geoscience*, *2*(7), 519-525. https://doi.org/10.1038/ngeo554

Schneider, U., Becker, A., Finger, P., Meyer-Christoffer, A., Rudolf, B., & Ziese, M. (2011). *GPCC full data reanalysis version 6.0 at 0.5◦: monthly land-surface precipita-tion from rain-gauges built on GTS-based and historic data*. Retrieved from: https://doi.org/10.5676/dwd_gpcc/fd_m_v6_050

Schnurrenberger, D., Russell, J., & Kelts, K. (2003). Classification of lacustrine sediments based on sedimentary components. *Journal of Paleolimnology*, *29*(2), 141-154. https://doi.org/10.1023/A:1023270324800

Stansell, N. D., Steinman, B. A., Abbott, M. B., Rubinov, M., & Roman-Lacayo, M. (2013). Lacustrine stable isotope record of precipitation changes in Nicaragua during the Little Ice Age and Medieval Climate Anomaly. *Geology*, *41*(2), 151-154. https://doi.org/10.1130/G33736.1

Stansell, N. D., Steinman, B. A., Lachniet, M. S., Feller, J., Harvey, W., Fernandez, A., et al. (2020). A lake sediment stable isotope record of late-middle to late Holocene hydroclimate variability in the western Guatemala highlands. *Earth and Planetary Science Letters*, *542*, 116327. https://doi.org/10.1016/j.epsl.2020.116327

Wang, C. (2007). Variability of the Caribbean Low-Level Jet and its relations to climate. *Climate Dynamics*, *29*(4), 411-422. https://doi.org/10.1007/s00382-007-0243-z

Waylen, P. R., Quesada, M. E., & Caviedes, C. N. (1996). Temporal and spatial variability of annual precipitation in Costa Rica and the Southern Oscillation. International Journal of Climatology, 16(2), 173-193. https://doi.org/10.1002/(SICI)1097-0088(199602)16:2<173::AID-JOC12>3.0.CO;2-R

Willmott, C. J., & Matsuura, K. (2001). *Terrestrial Air Temperature and Precipitation: Monthly and Annual Time Series (1950–1999), Version 5.0.1. Center for Climatic Research*. Retrieved from: http://climate.geog.udel.edu/~climate/html_pages/README.ghcn_ts2.html

Winter, A., Zanchettin, D., Lachniet, M., Vieten, R., Pausata, F. S. R., Ljungqvist, F. C., et al. (2020). Initiation of a stable convective hydroclimatic regime in Central America circa

9000 years BP. *Nature Communications, 11*(1), 716. https://doi.org/10.1038/s41467-020-14490-y

Paleoceanography and Paleoclimatology

Supporting Information for

Incoherency in Central American hydroclimate proxy records spanning the last millennium

Jonathan Obrist-Farner[1], Byron Steinman[2], Nathan Stansell[3], and Jeremy Maurer[1]

1. Geosciences and Geological and Petroleum Engineering Department, Missouri University of Science and Technology, USA.
2. Large Lakes Observatory and Department of Earth and Environmental Sciences, University of Minnesota Duluth, USA.
3. Department of Geology and Environmental Geosciences, Northern Illinois University, USA.

Contents of this file

Figures S1 to S27

Additional Supporting Information (Files uploaded separately)

Tables S1. Radiocarbon dates for the core from Lake Petén Itzá.
Table S2. Radiocarbon dates for the core from Lake Izabal.
Table S3. Elemental abundances for the Petén Itzá core in counts per second.
Table S4. Elemental abundances for the Izabal core in counts per second.

Introduction

This document contains supplementary figures and references as supporting information. Additional data tables are provided as separate excel files. The methodology used to generate the following figures is described in the main text of the manuscript.

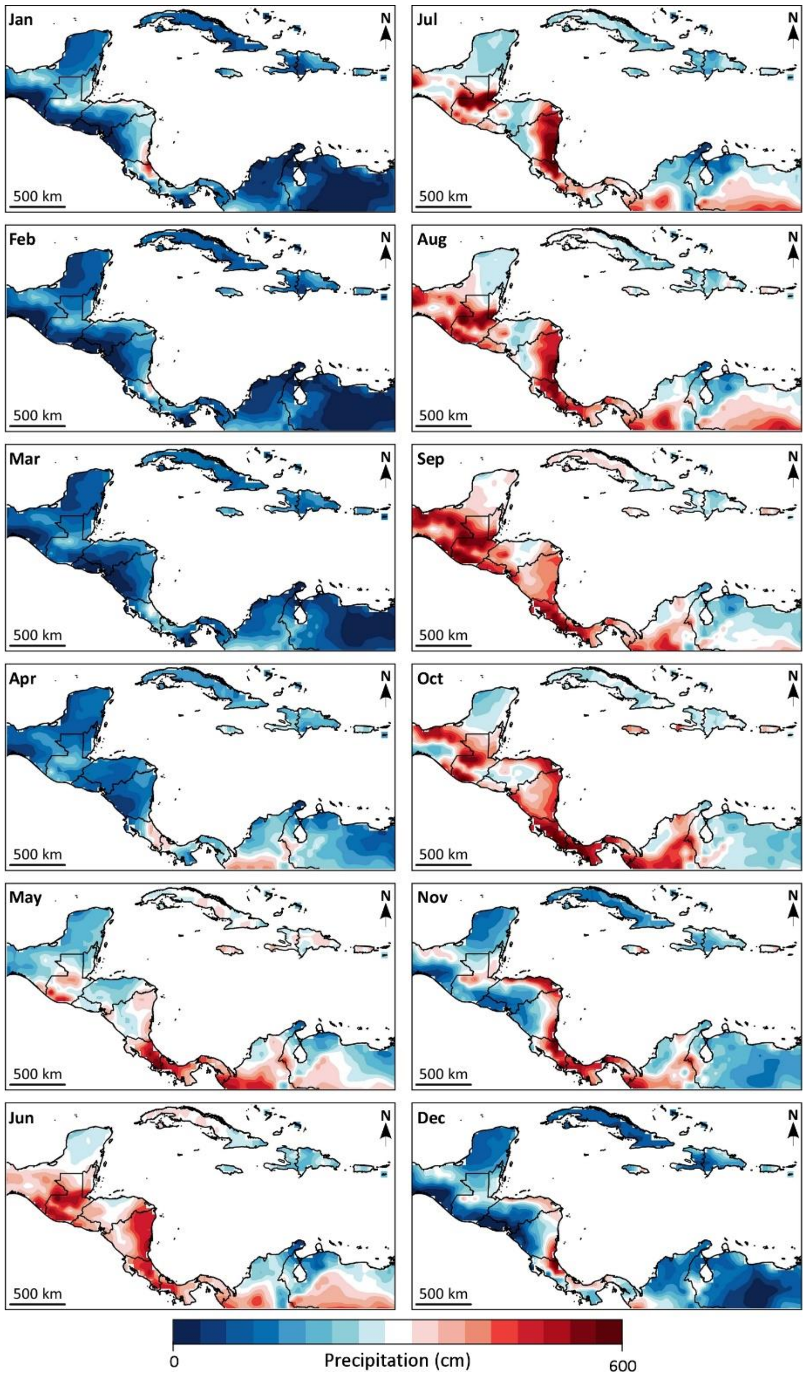

Figure S1. Maps of Central America, the Caribbean, and northern South America showing mean monthly precipitation based on three gridded data products (Willmott & Matsuura, 2001; Schneider et al., 2011; Harris et al., 2014) spanning the period 1966-2016 CE.

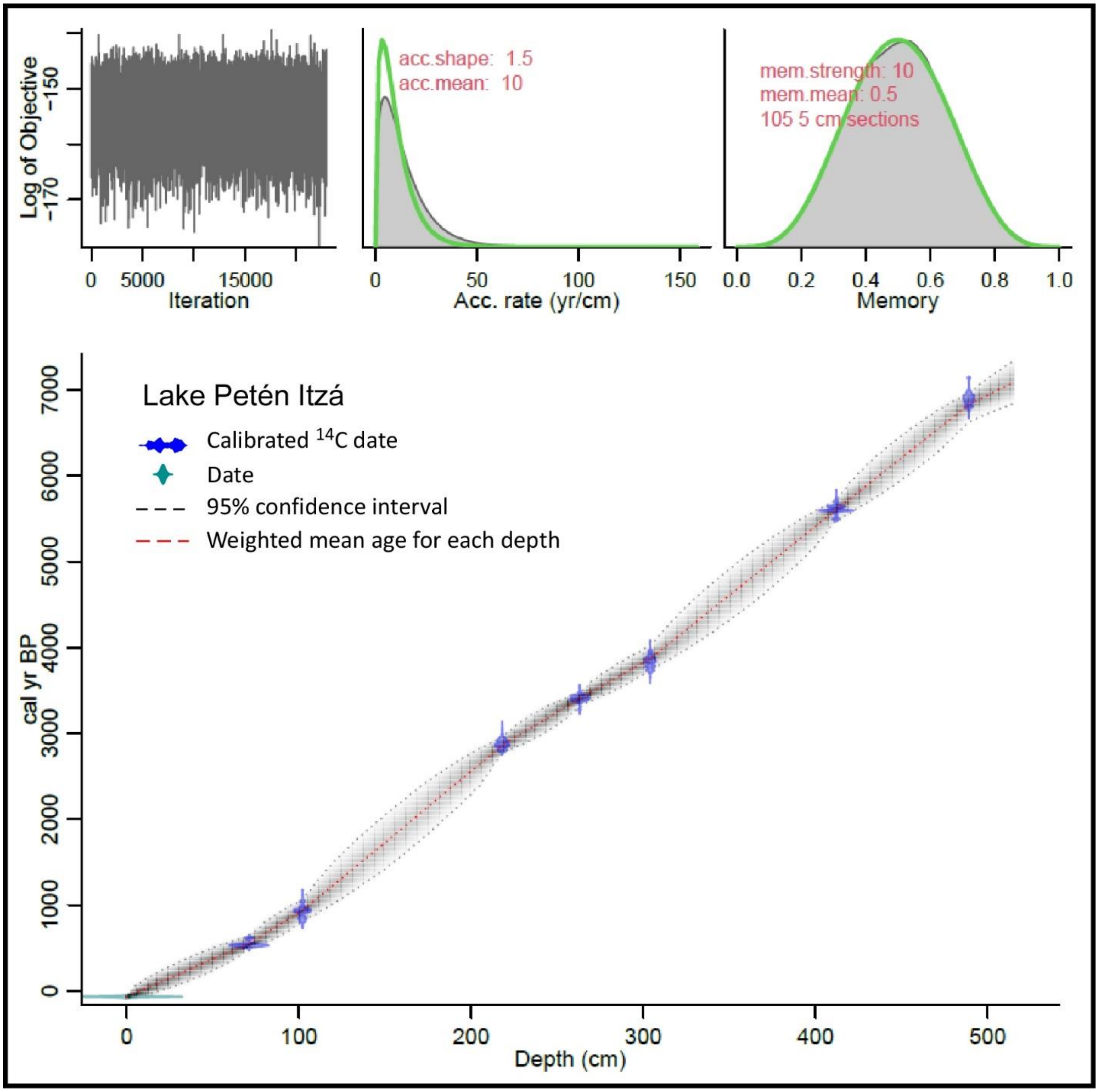

Figure S2. Age-depth model for Lake Petén Itzá (this study; Obrist-Farner & Rice, 2019). All radiocarbon dates were obtained from charcoal/wood fragments. Red line shows the best-fit model based on weighted mean ages, and stippled gray lines show 95% confidence intervals. All dates were calibrated using IntCal20 (Reimer et al., 2020). The age-depth model was generated using Bacon (Blaauw & Christen, 2011). Raw data provided in supplementary table 1.

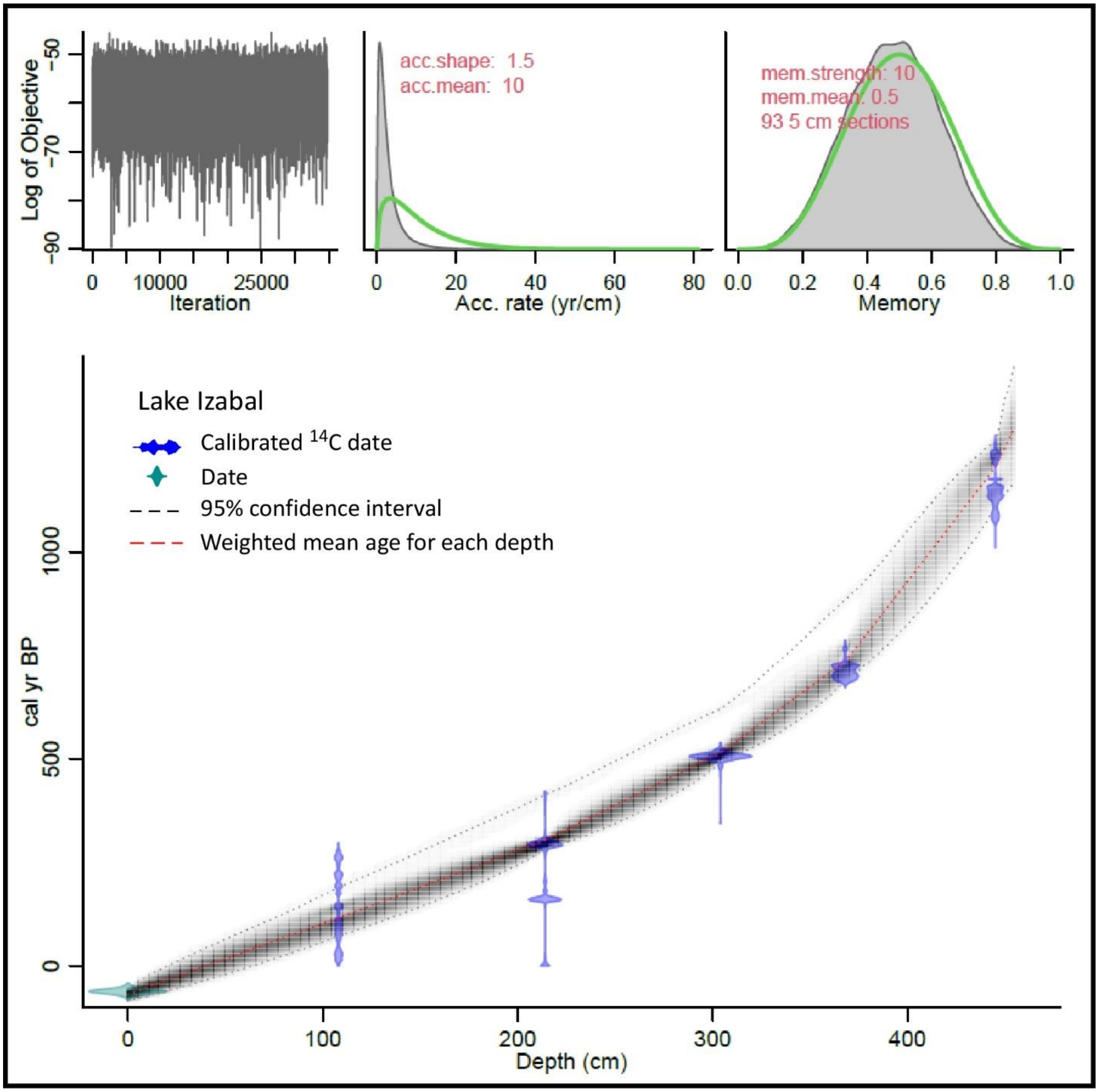

Figure S3. Age-depth model for Lake Izabal (this study; Hernández et al., 2020). All radiocarbon dates were obtained from charcoal/wood fragments. Red line shows the best-fit model based on weighted mean ages, and stippled gray lines show 95% confidence intervals. All dates were calibrated using IntCal20 (Reimer et al., 2020). The age-depth model was generated using Bacon (Blaauw & Christen, 2011). Raw data provided in supplementary table 2.

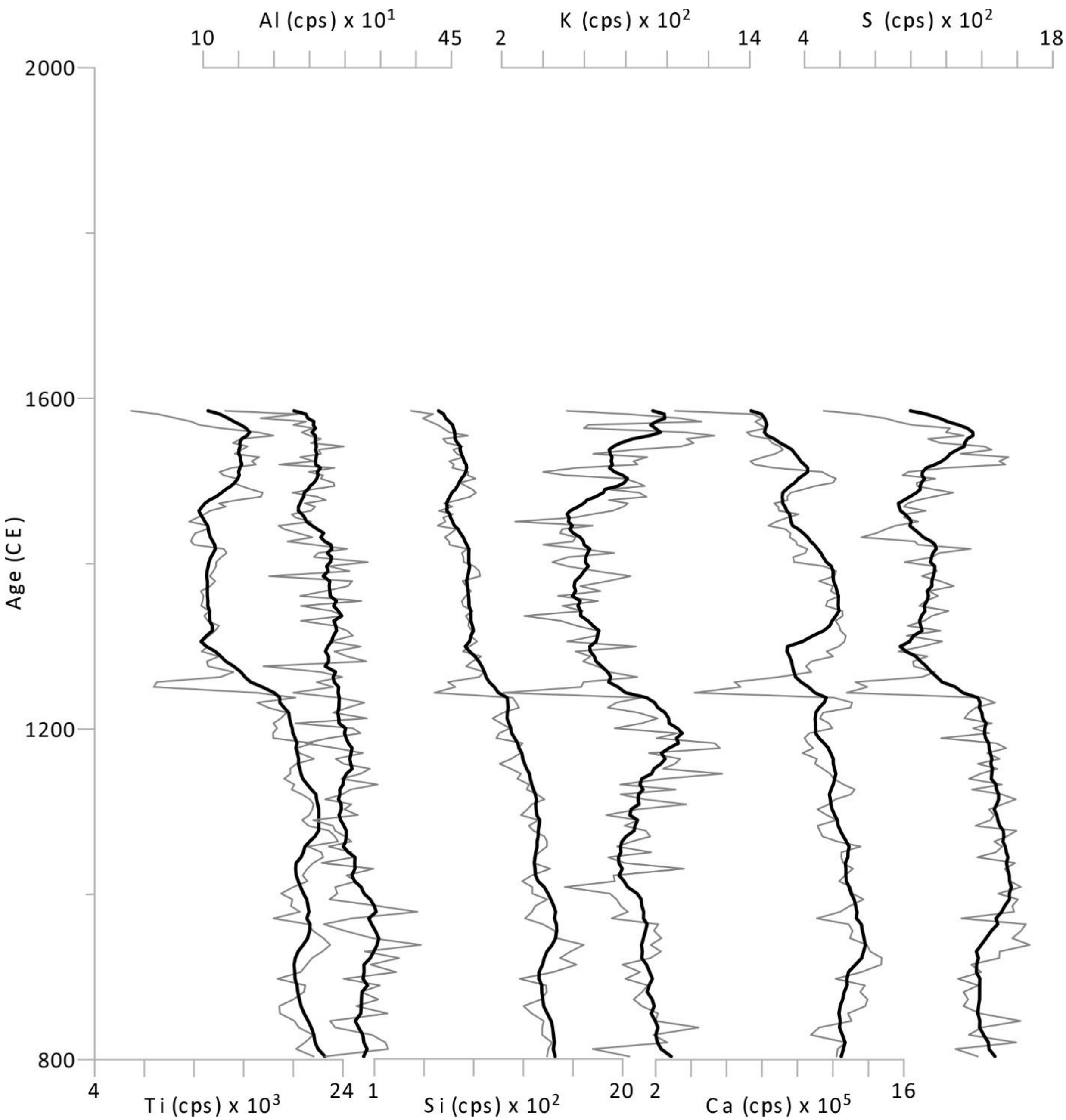

Figure S4. Proxy data versus age for the Lake Petén Itzá core. Figure shows elemental abundances in counts per second (cps). The gray line shows the unfiltered data and the black lines show the 10 point moving average. Raw data provided in supplementary table 3.

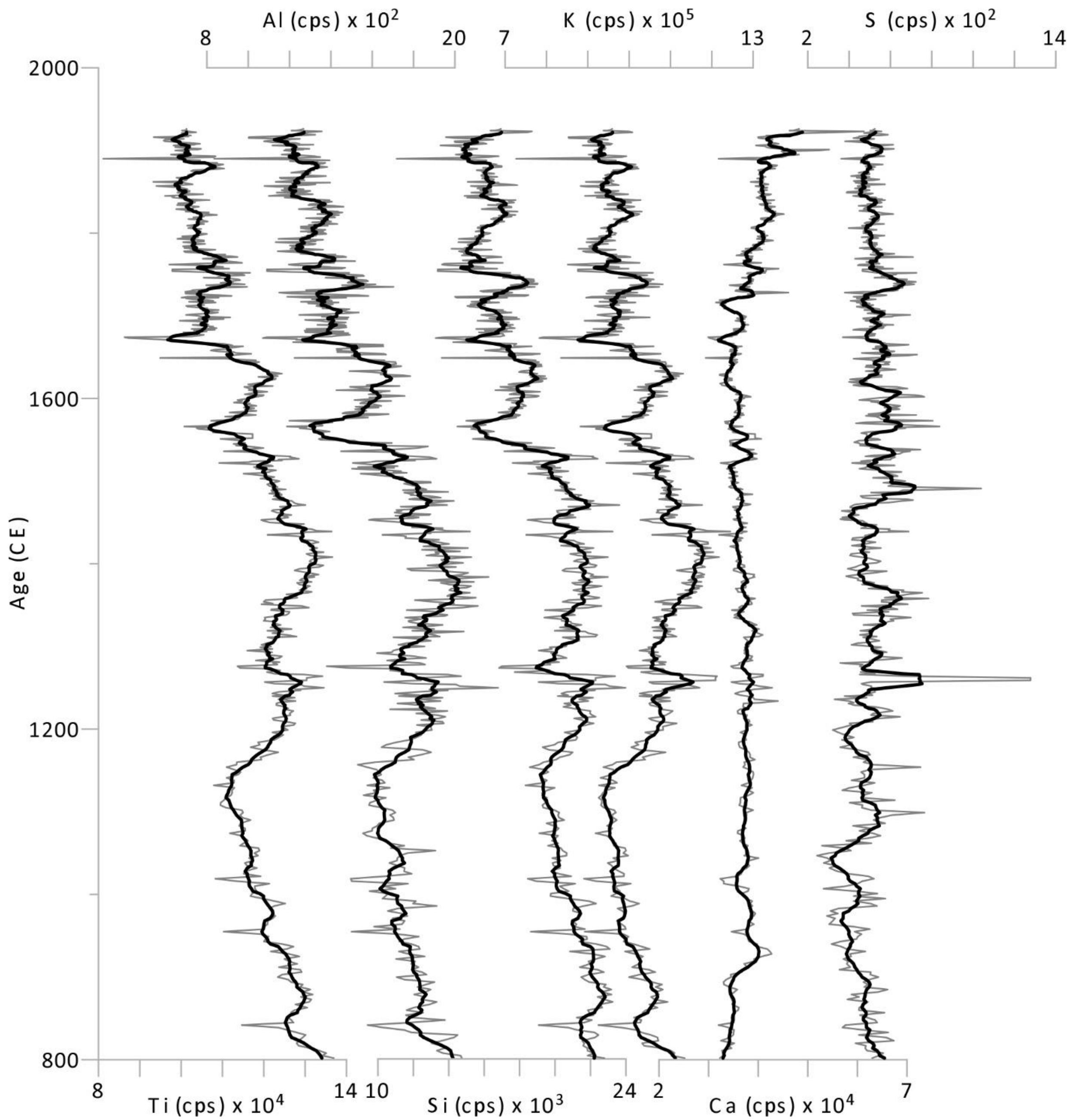

Figure S5. Proxy data versus age for the Lake Izabal core. Figure shows elemental abundances in counts per second (cps). The gray line shows the unfiltered data and the black lines show the 10 point moving average. Raw data provided in supplementary table 4.

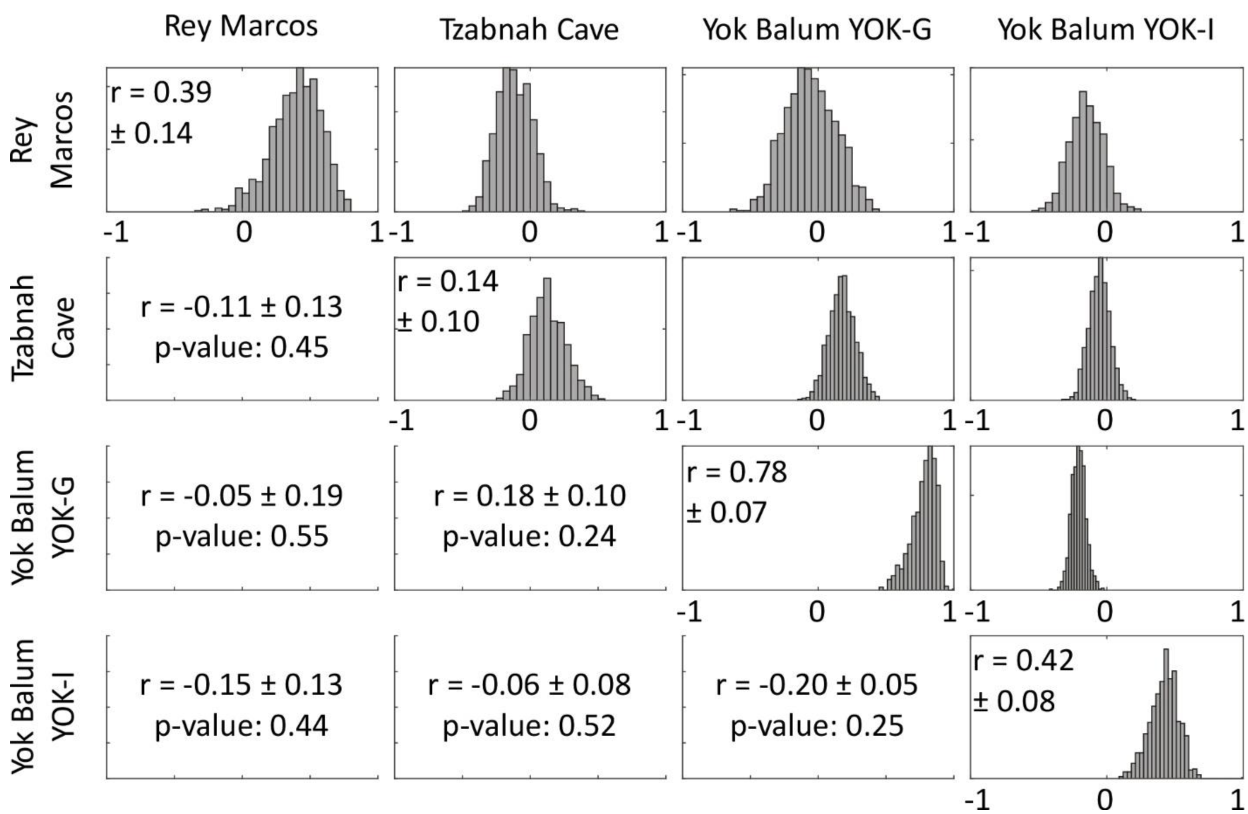

Figure S6. Matrix showing the range of correlation values (upper right) for all speleothem record realizations used in this study utilizing 1000 age-proxy pairs. The diagonal quantifies the uncertainties in the age-depth model; for example, an age-depth model with no uncertainty would have correlation equal to 1. The distribution represents how correlated the 1000 age-proxy realizations are to each other (see Supplementary Material). The lower left shows mean correlation values, ±1σ, and mean p-values for the records analyzed. The $\delta^{18}O$ records been multiplied by negative one so that positive correlation indicates consistent behavior between proxy sites.

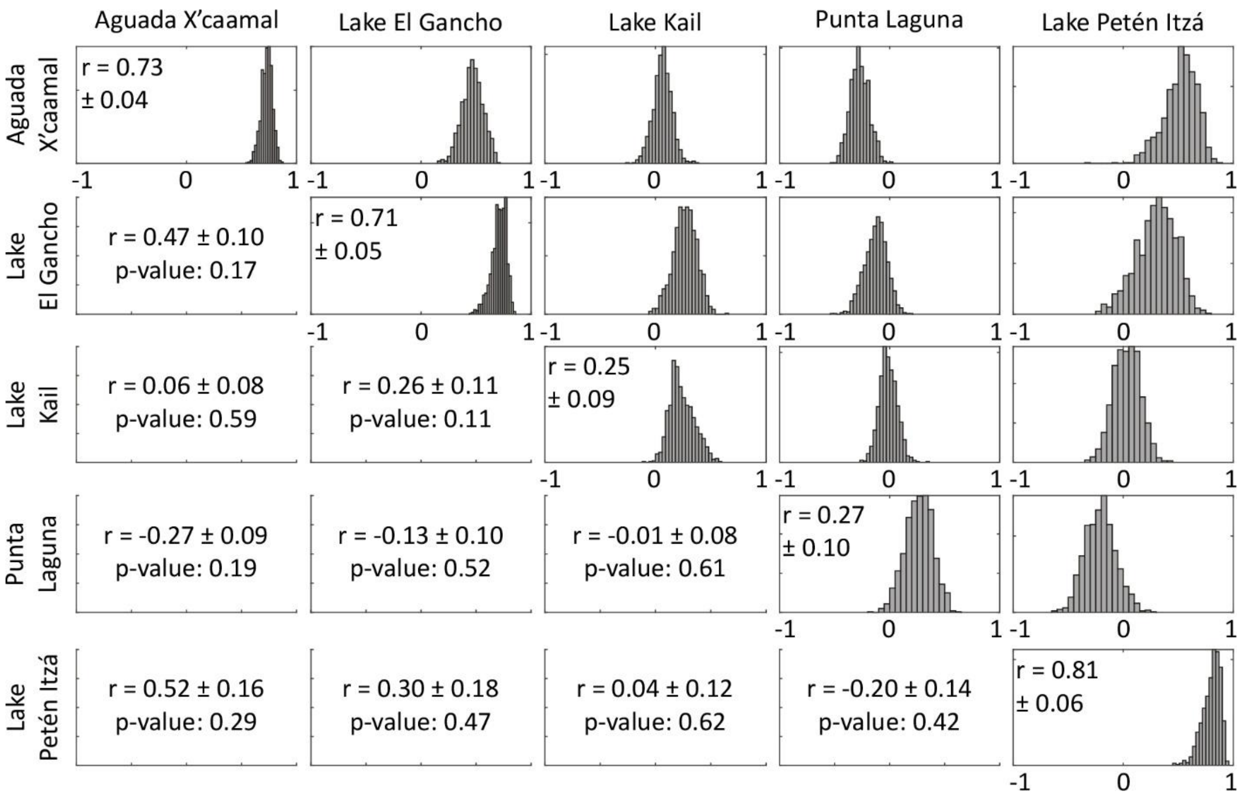

Figure S7. Matrix showing the range of correlation values (upper right) for all small and closed lacustrine basin record realizations used in this study utilizing 1000 age-proxy pairs. The diagonal quantifies the uncertainties in the age-depth model; for example, an age-depth model with no uncertainty would have correlation equal to 1. The distribution represents how correlated the 1000 age-proxy realizations are to each other (see Supplementary Material). The lower left shows mean correlation values, ±1σ, and mean p-values for the records analyzed. The $\delta^{18}O$ records been multiplied by negative one so that positive correlation indicates consistent behavior between proxy sites.

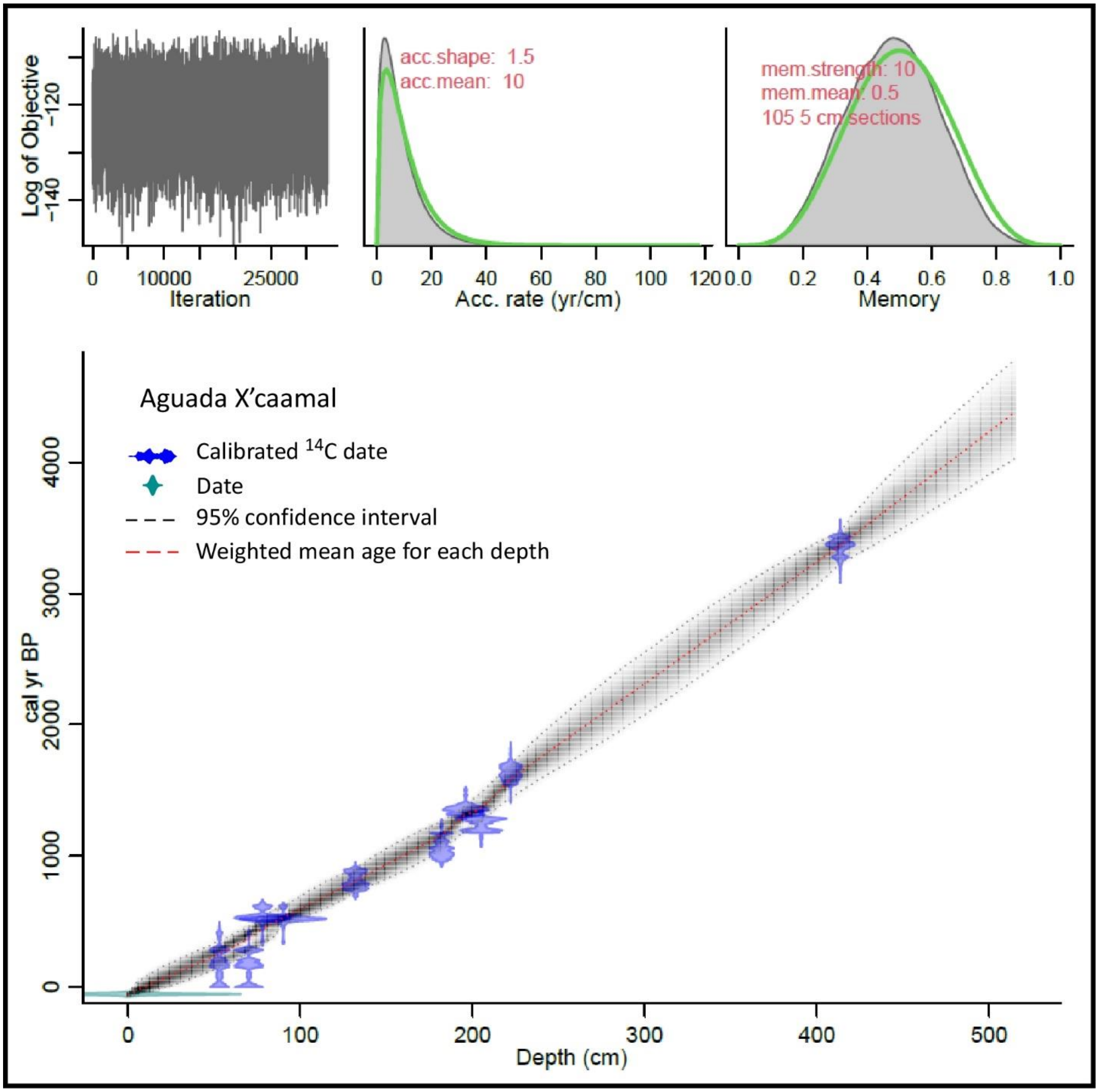

Figure S8. Age-depth model for Aguada X'caamal (Hodell et al., 2005). All radiocarbon dates are from terrestrial organic material. Red line shows the best-fit model based on weighted mean ages, and stippled gray lines show 95% confidence intervals. All dates were calibrated using IntCal20 (Reimer et al., 2020). The age-depth model was generated using Bacon (Blaauw & Christen, 2011).

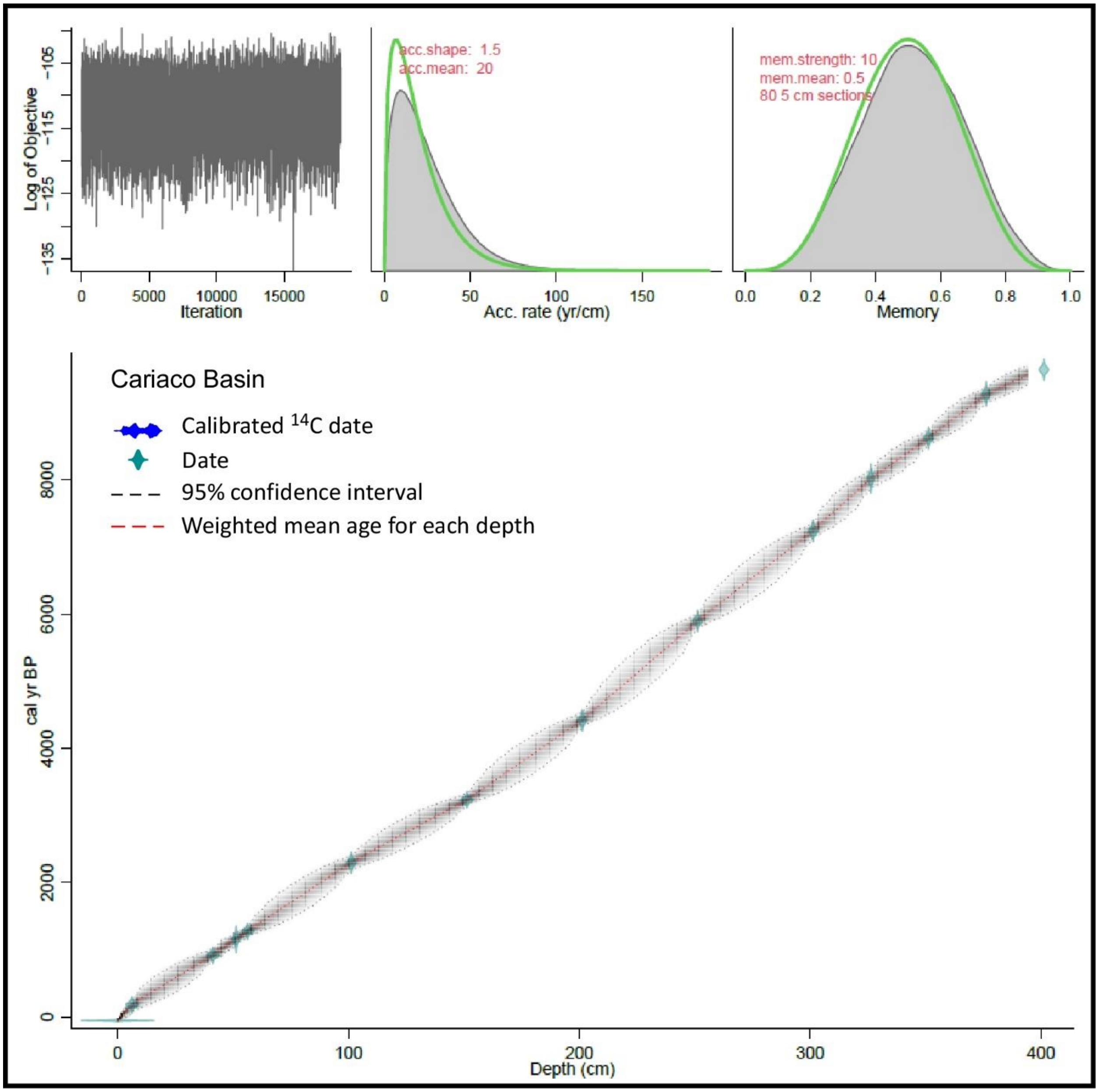

Figure S9. Age-depth model for the Cariaco Basin sediment core (Haug et al., 2001). All radiocarbon dates are from planktic foraminifera and corrected from the marine reservoir effect. Red line shows the best-fit model based on weighted mean ages, and stippled gray lines show 95% confidence intervals. The age-depth model was generated using Bacon (Blaauw & Christen, 2011).

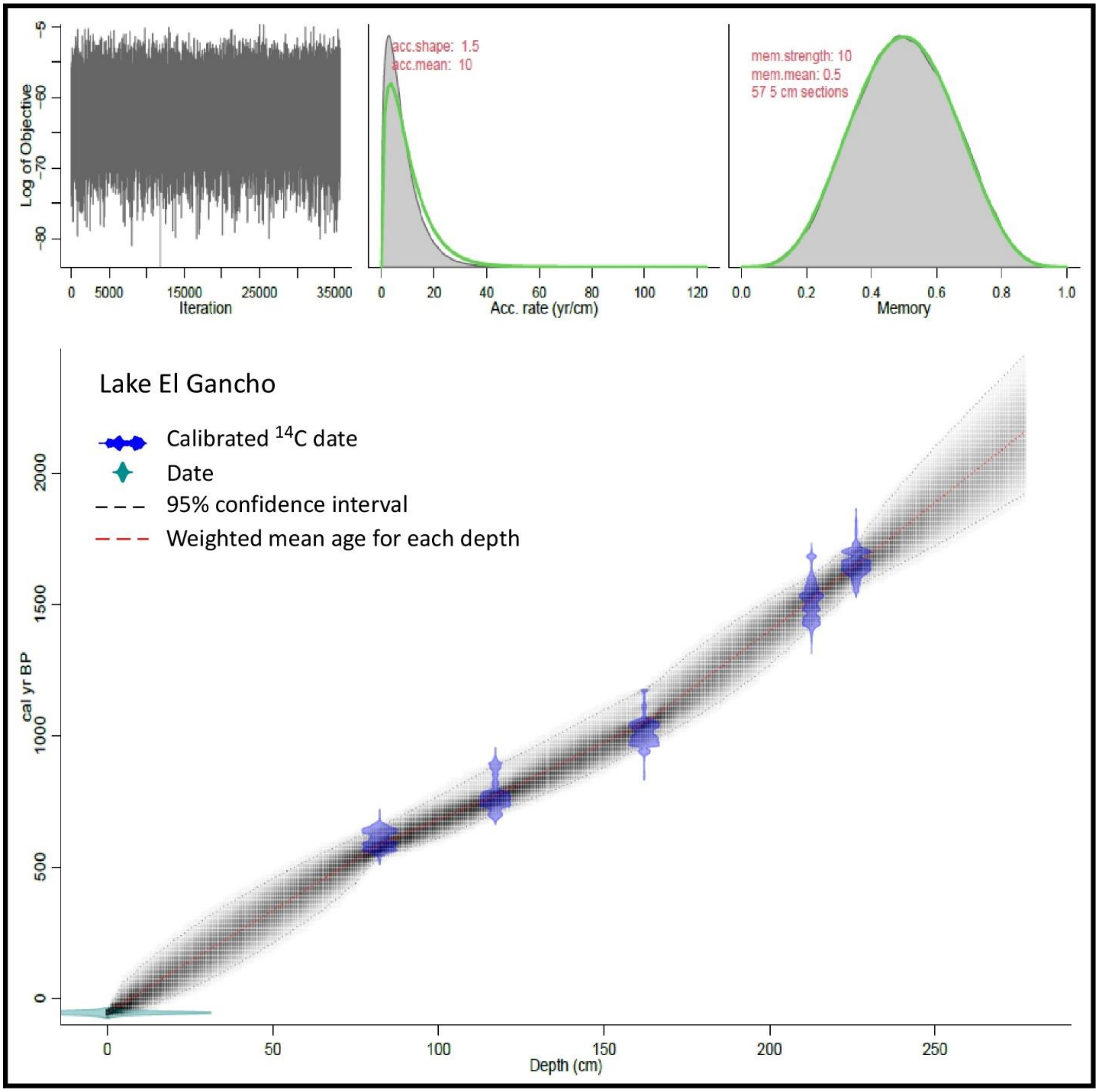

Figure S10. Age-depth model for Lake El Gancho (Stansell et al., 2013). All radiocarbon dates were obtained from charcoal fragments. Red line shows the best-fit model based on weighted mean ages, and stippled gray lines show 95% confidence intervals. All dates were calibrated using IntCal20 (Reimer et al., 2020). The age-depth model was generated using Bacon (Blaauw & Christen, 2011).

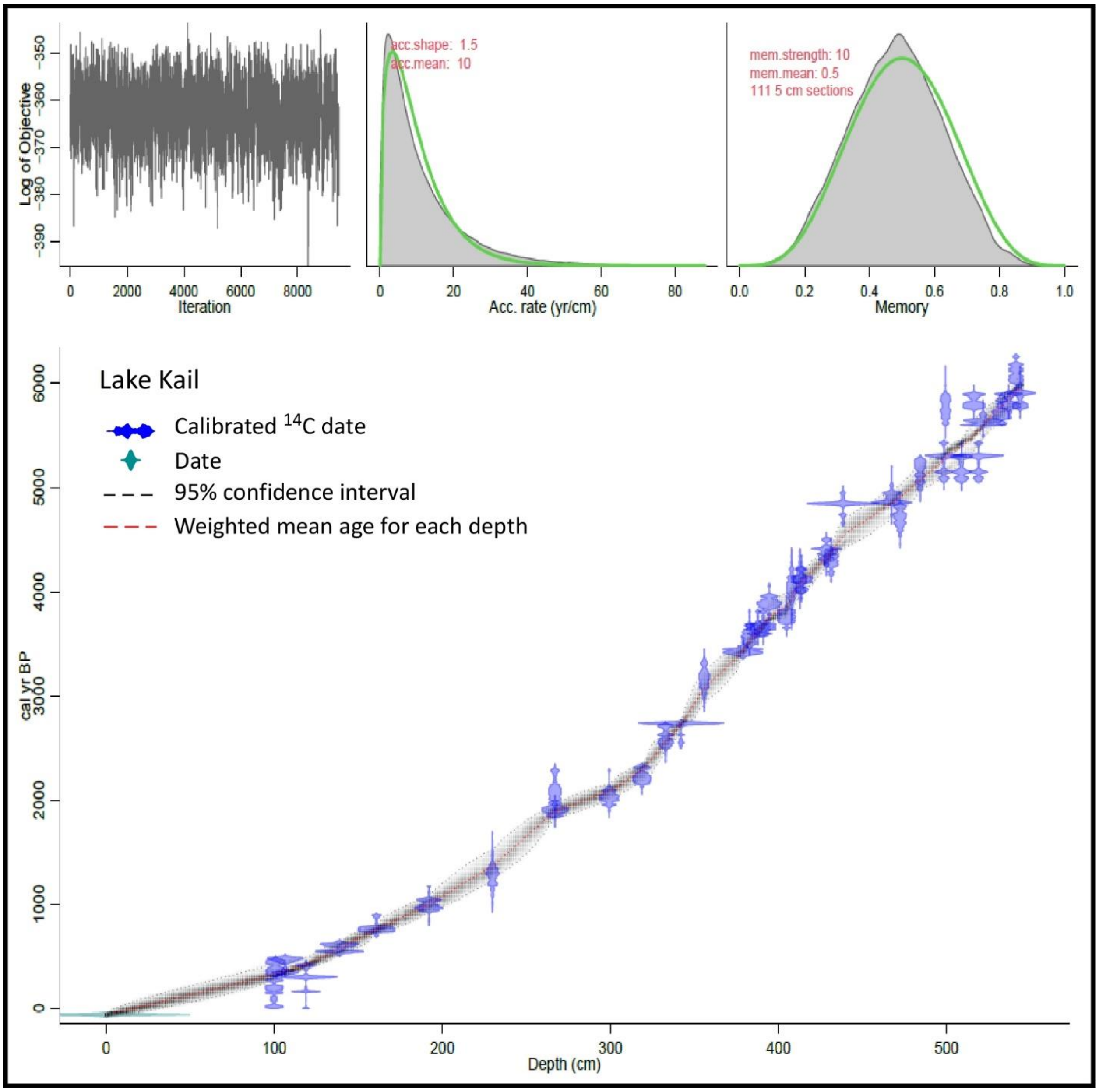

Figure S11. Age-depth model for Lake Kail (Stansell et al., 2020). All radiocarbon dates were obtained from charcoal and leaf fragments. Red line shows the best-fit model based on weighted mean ages, and stippled gray lines show 95% confidence intervals. All dates were calibrated using IntCal20 (Reimer et al., 2020). The age-depth model was generated using Bacon (Blaauw & Christen, 2011).

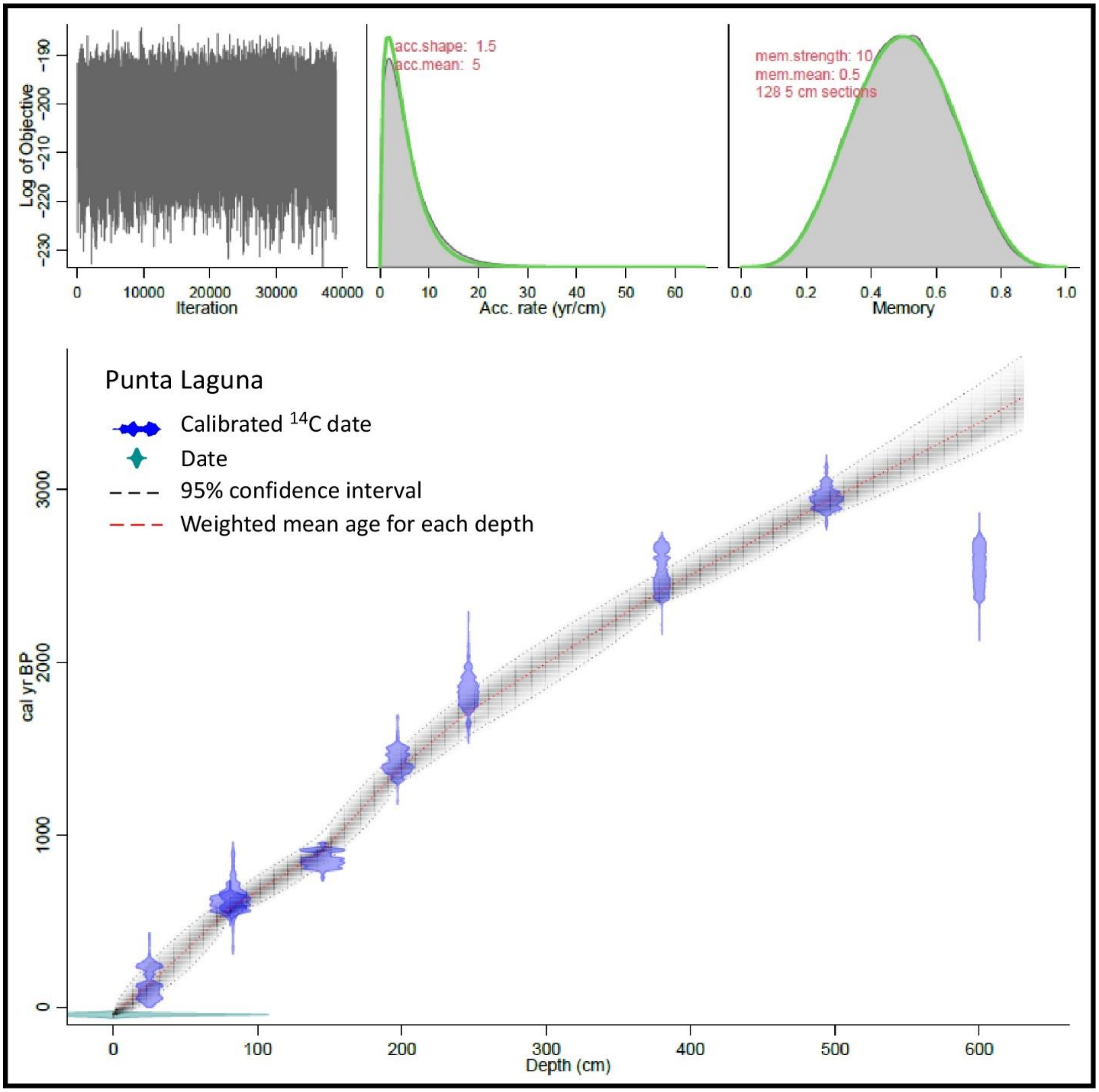

Figure S12. Age-depth model for Punta Laguna (Curtis et al., 1996). Radiocarbon dates were obtained from five terrestrial wood samples and four from shell material. Shell radiocarbon dates were corrected for hard water lake error for Punta Laguna. Red line shows the best-fit model based on weighted mean ages, and stippled gray lines show 95% confidence intervals. All dates were calibrated using IntCal20 (Reimer et al., 2020). The age-depth model was generated using Bacon (Blaauw & Christen, 2011).

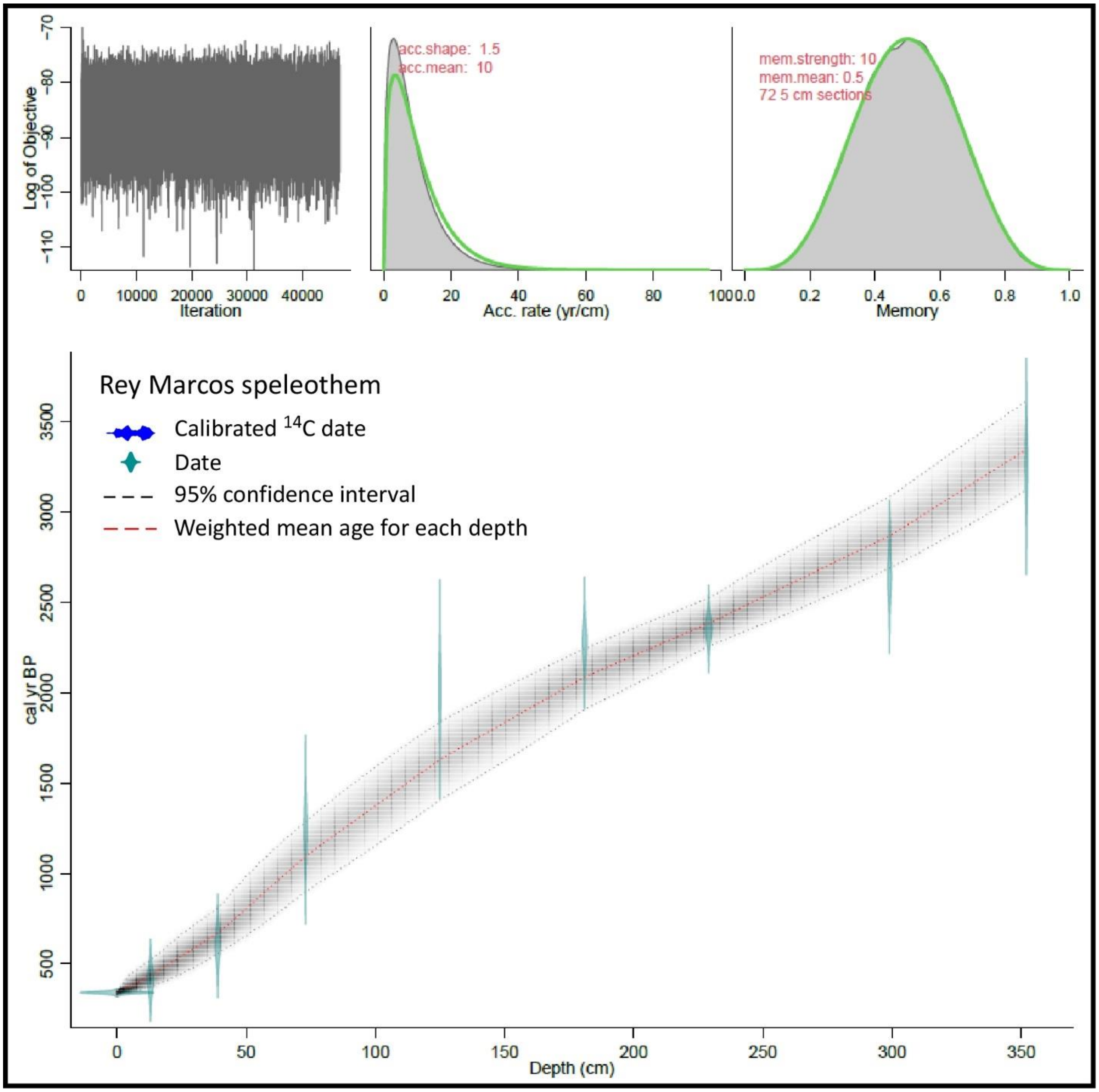

Figure S13. Age-depth model for the Rey Marcos speleothem (Winter et al., 2020). The age model is based on 21 U/Th dates. radiocarbon dates were obtained from charcoal/wood fragments. Red line shows the best-fit model based on weighted mean ages, and stippled gray lines show 95% confidence intervals. The age-depth model was generated using Bacon (Blaauw & Christen, 2011). Model generated is only for the first 4000 years of the record.

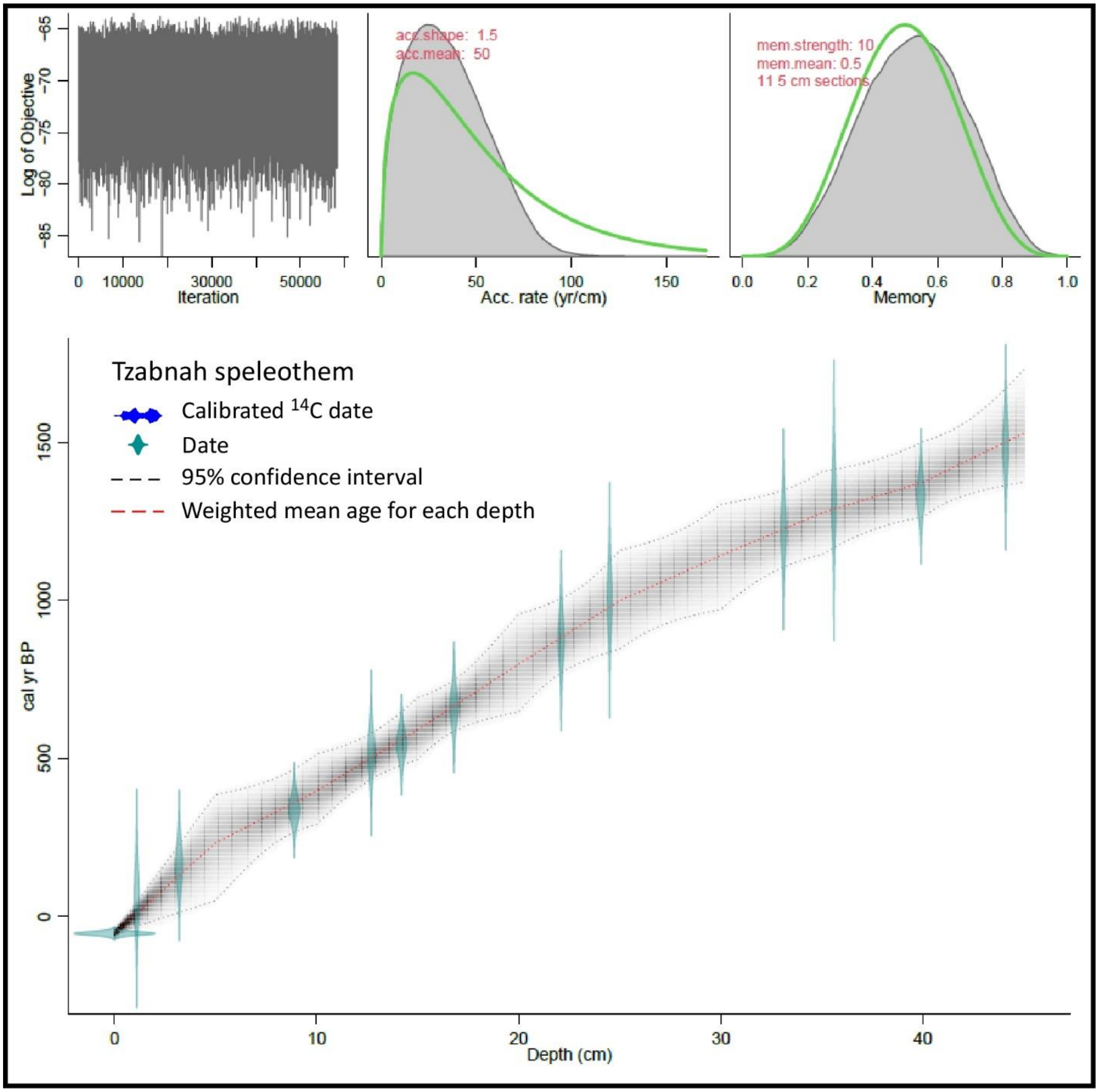

Figure S14. Age-depth model for the Tzabnah speleothem (Medina-Elizalde et al., 2010). The age model is based on 12 U/Th dates. Red line shows the best-fit model based on weighted mean ages, and stippled gray lines show 95% confidence intervals. The age-depth model was generated using Bacon (Blaauw & Christen, 2011).

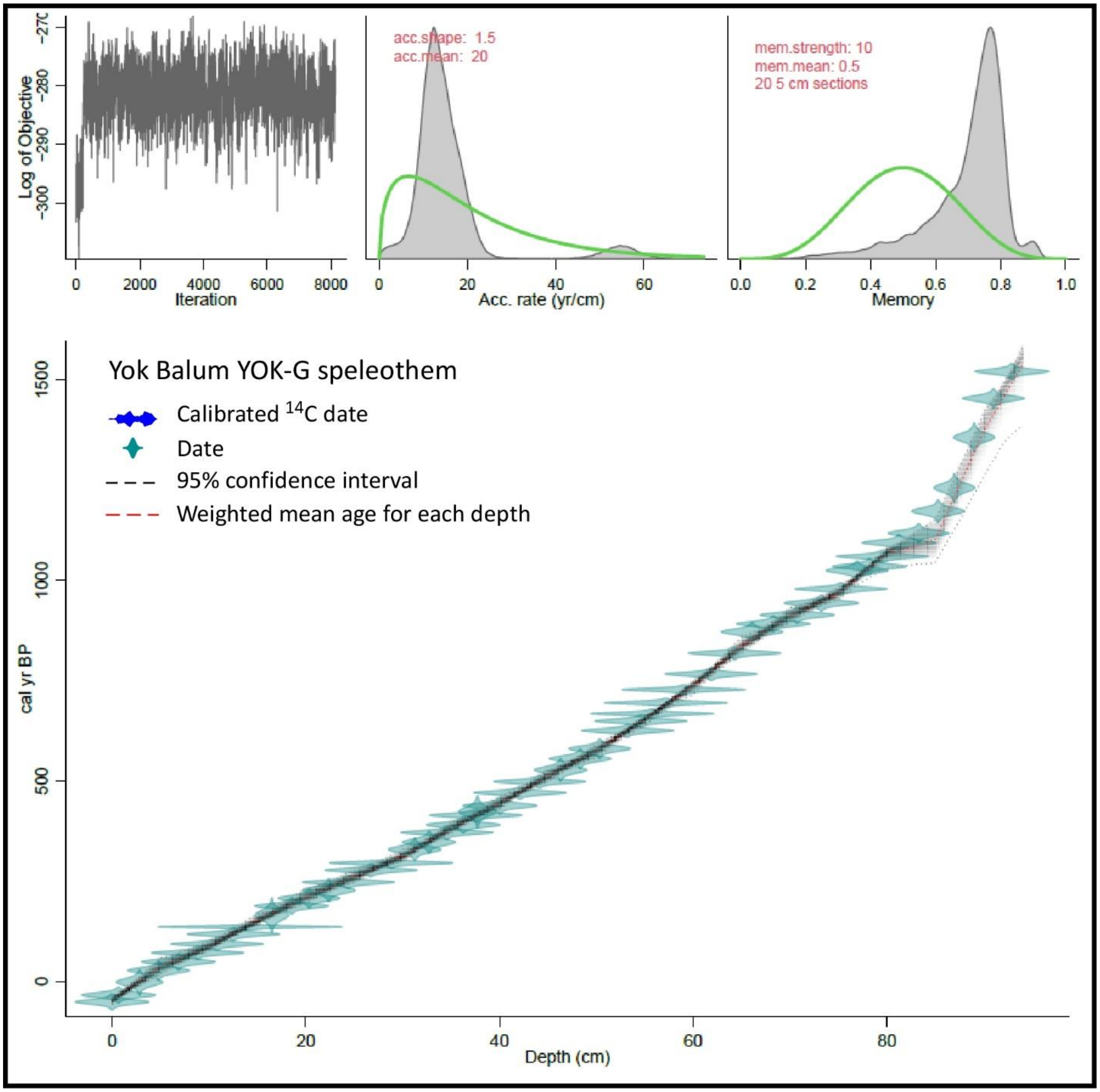

Figure S15. Age-depth model for the YOK-G speleothem (Asmerom et al., 2020). The age model is based on 52 U/Th dates. Red line shows the best-fit model based on weighted mean ages, and stippled gray lines show 95% confidence intervals. The age-depth model was generated using Bacon (Blaauw & Christen, 2011).

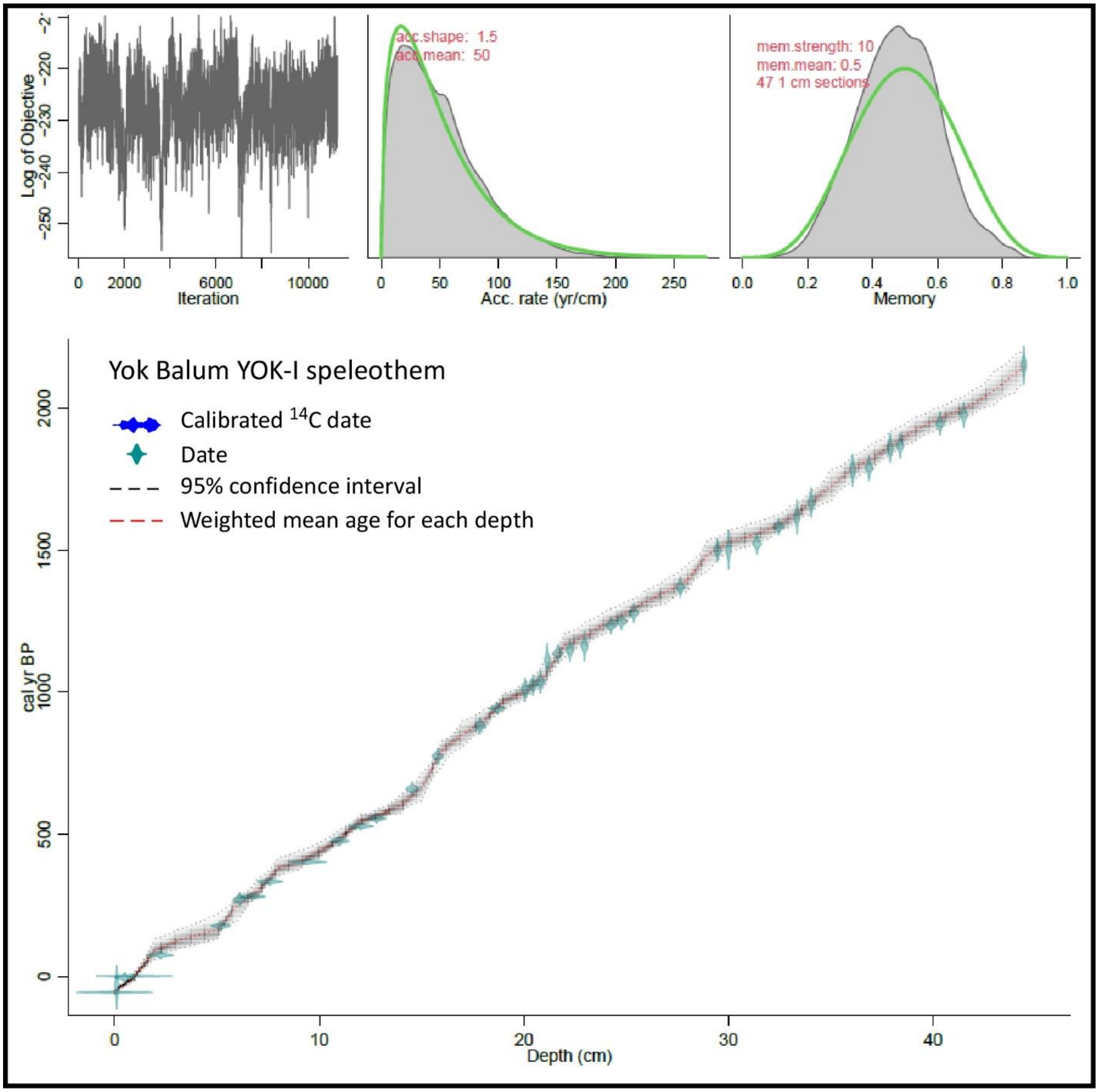

Figure S16. Age-depth model for YOK-I (Kennett et al., 2012). The age model is based on 40 U/Th dates. Red line shows the best-fit model based on weighted mean ages, and stippled gray lines show 95% confidence intervals. The age-depth model was generated using Bacon (Blaauw & Christen, 2011).

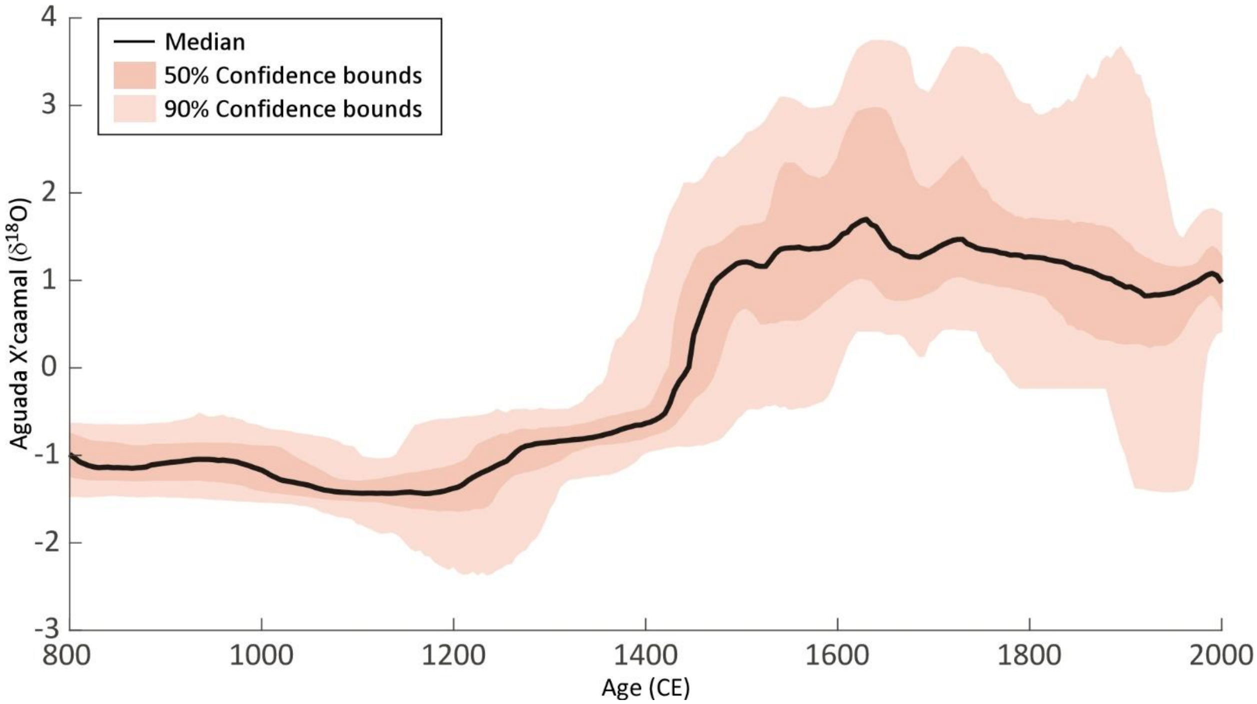

Figure S17. Median, 50% and 90% confidence bounds for the Aguada X'caamal $\delta^{18}O$ record (Hodell et al., 2005). The plot shows the range of proxy values for 1000 age-depth models (same set of models used for the correlation analysis shown in Figure 5). Note that the graph shows the unconditional probability at each time step. That is, the graph does not represent correlations between time steps.

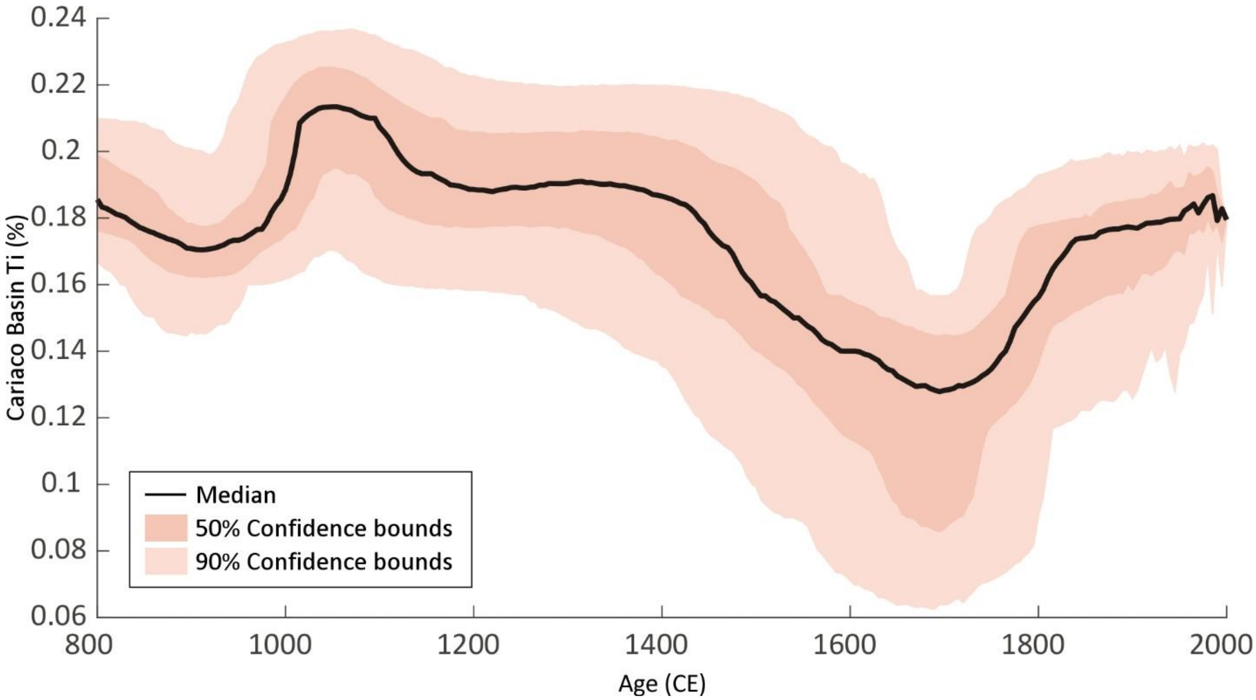

Figure S18. Median, 50% and 90% confidence bounds for the Cariaco Basin titanium record (Haug et al., 2001). The plot shows the range of proxy values for 1000 age-depth models (same set of models used for the correlation analysis shown in Figure 5). Note that the graph shows the unconditional probability at each time step. That is, the graph does not represent correlations between time steps.

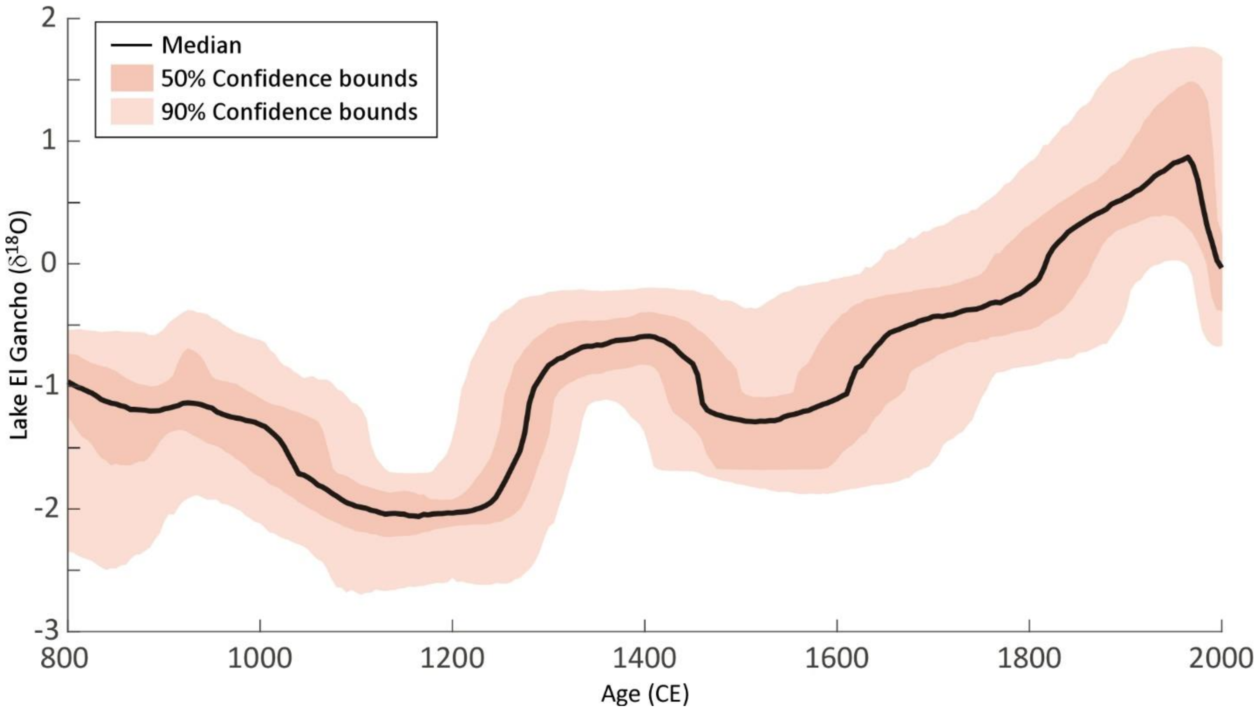

Figure S19. Median, 50% and 90% confidence bounds for the Lake El Gancho δ^{18}O record (Stansell et al., 2013). The plot shows the range of proxy values for 1000 age-depth models (same set of models used for the correlation analysis shown in Figure 5). Note that the graph shows the unconditional probability at each time step. That is, the graph does not represent correlations between time steps.

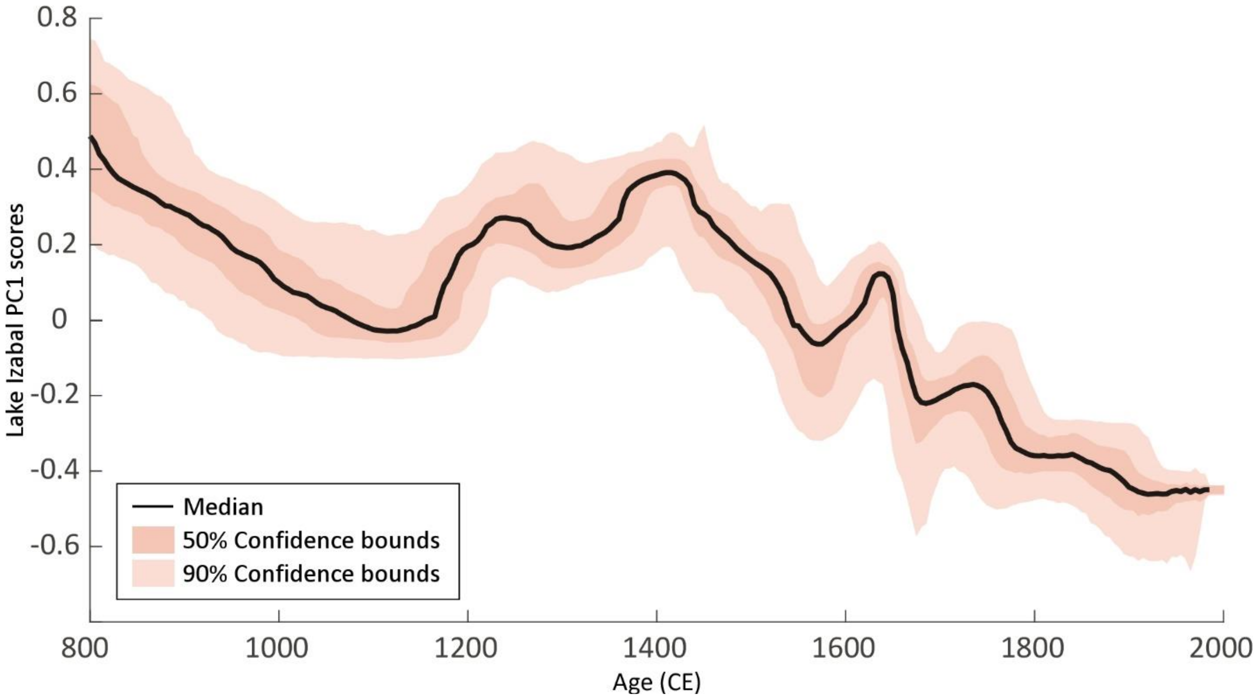

Figure S20. Median, 50% and 90% confidence bounds for the Lake Izabal PC1 scores (this study). The plot shows the range of proxy values for 1000 age-depth models (same set of models used for the correlation analysis shown in Figure 5). Note that the graph shows the unconditional probability at each time step. That is, the graph does not represent correlations between time steps.

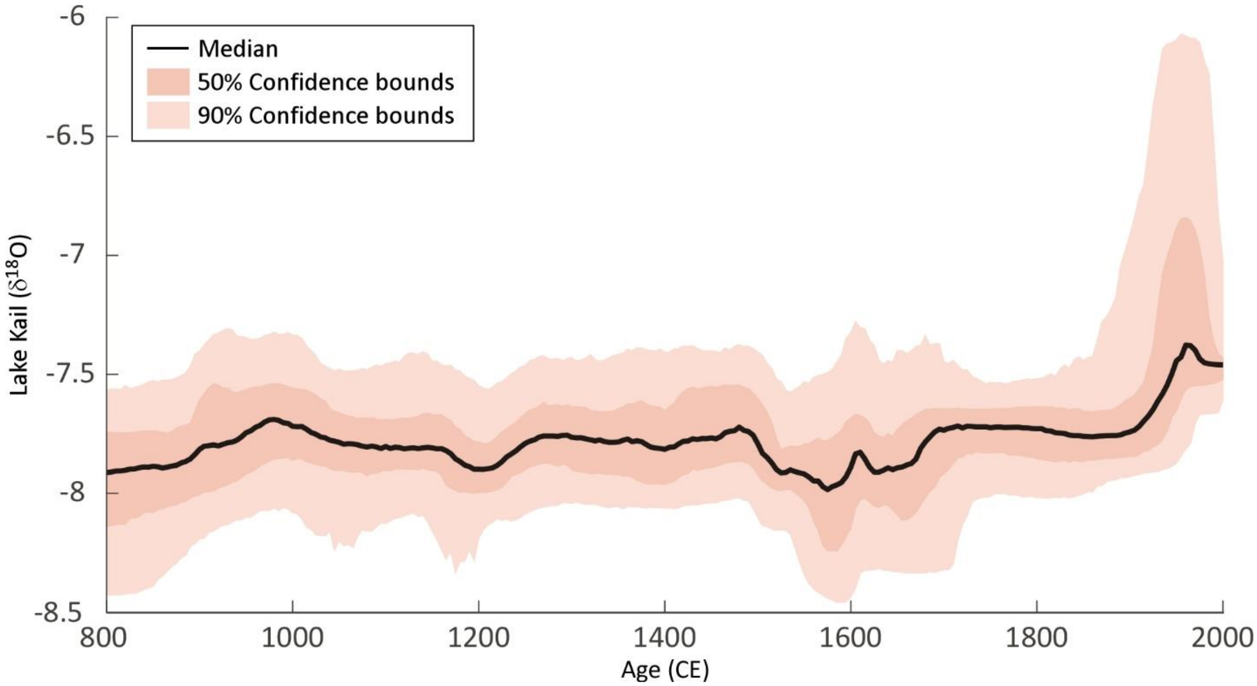

Figure S21. Median, 50% and 90% confidence bounds for the Lake Kail $\delta^{18}O$ record (Stansell et al., 2020). The plot shows the range of proxy values for 1000 age-depth models (same set of models used for the correlation analysis shown in Figure 5). Note that the graph shows the unconditional probability at each time step. That is, the graph does not represent correlations between time steps.

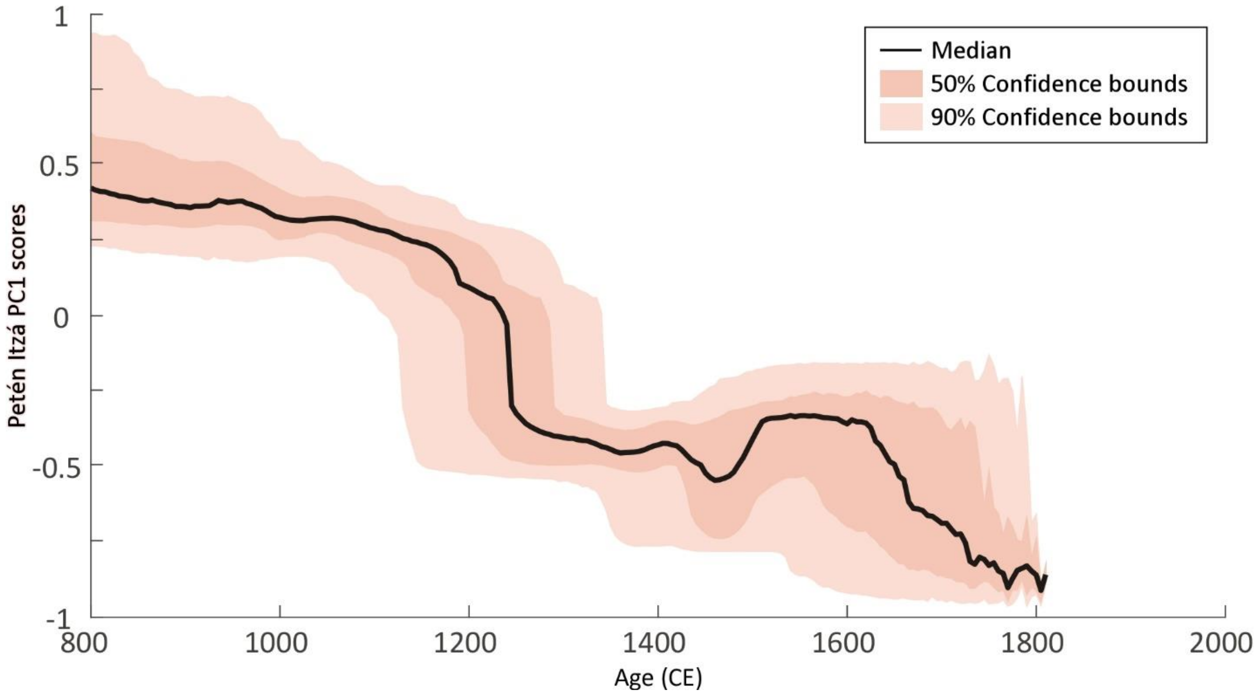

Figure S22. Median, 50% and 90% confidence bounds for the Lake Petén Itzá PC1 scores (this study). The plot shows the range of proxy values for 1000 age-depth models (same set of models used for the correlation analysis shown in Figure 5). Note that the graph shows the unconditional probability at each time step. That is, the graph does not represent correlations between time steps.

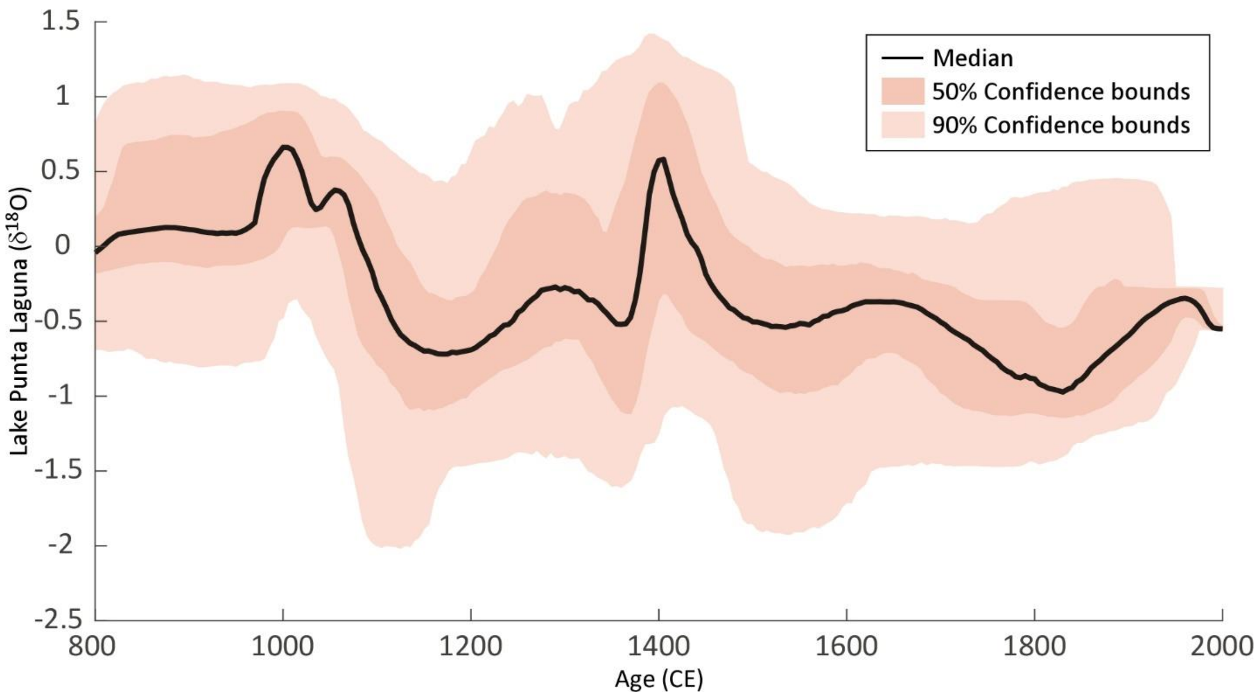

Figure S23. Median, 50% and 90% confidence bounds for the Punta Laguna $\delta^{18}O$ record (Curtis et al., 1996). The plot shows the range of proxy values for 1000 age-depth models (same set of models used for the correlation analysis shown in Figure 5). Note that the graph shows the unconditional probability at each time step. That is, the graph does not represent correlations between time steps.

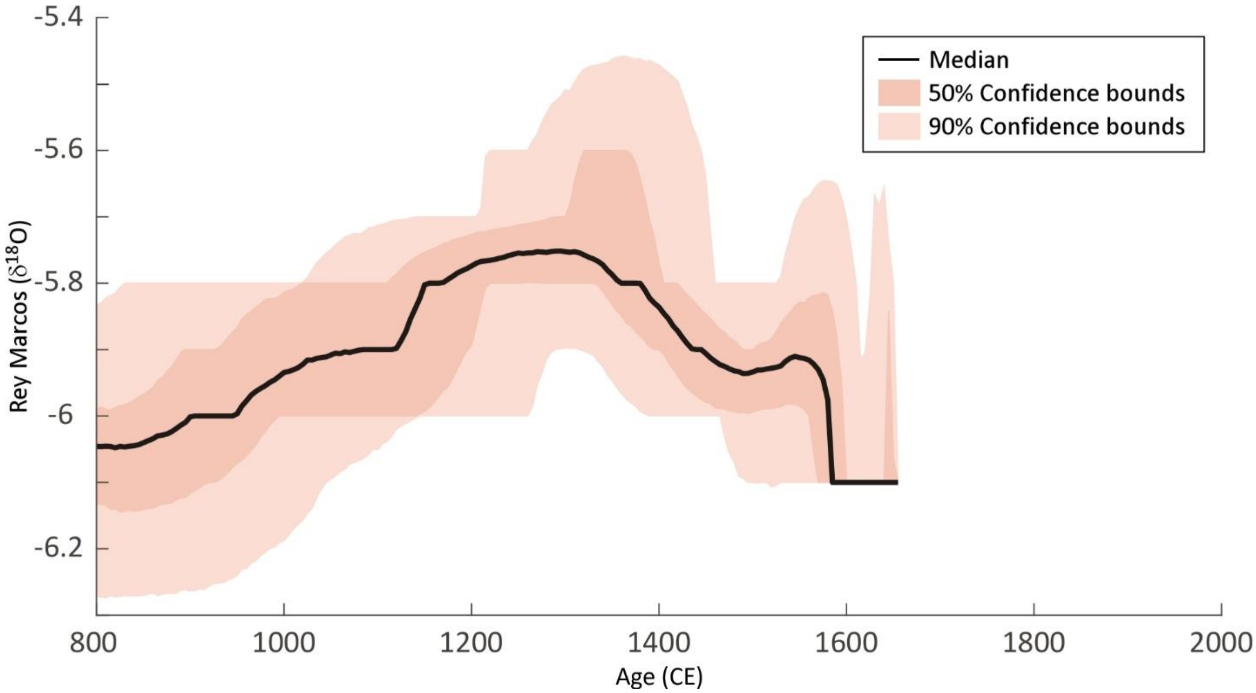

Figure S24. Median, 50% and 90% confidence bounds for the Rey Marcos speleothem $\delta^{18}O$ record (Winter et al., 2020). The plot shows the range of proxy values for 1000 age-depth models (same set of models used for the correlation analysis shown in Figure 5). Note that the graph shows the unconditional probability at each time step. That is, the graph does not represent correlations between time steps.

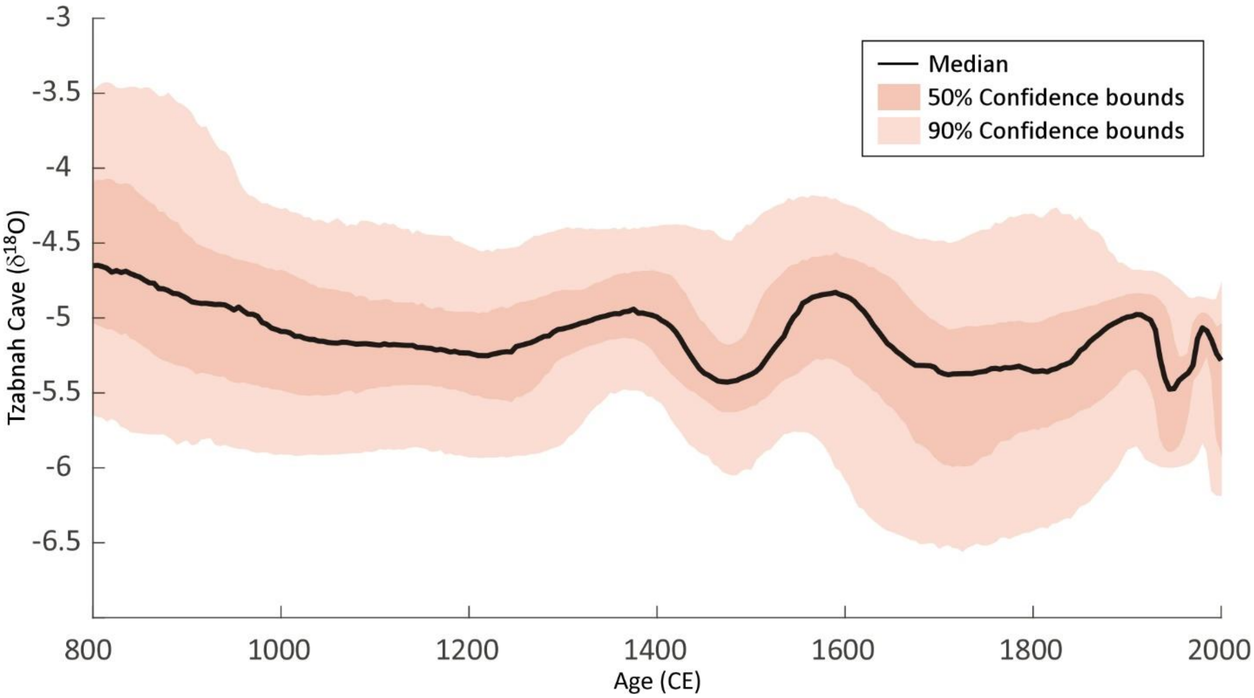

Figure S25. Median, 50% and 90% confidence bounds for the Tzabnah Cave speleothem $\delta^{18}O$ record (Medina-Elizalde et al., 2010). The plot shows the range of proxy values for 1000 age-depth models (same set of models used for the correlation analysis shown in Figure 5). Note that the graph shows the unconditional probability at each time step. That is, the graph does not represent correlations between time steps.

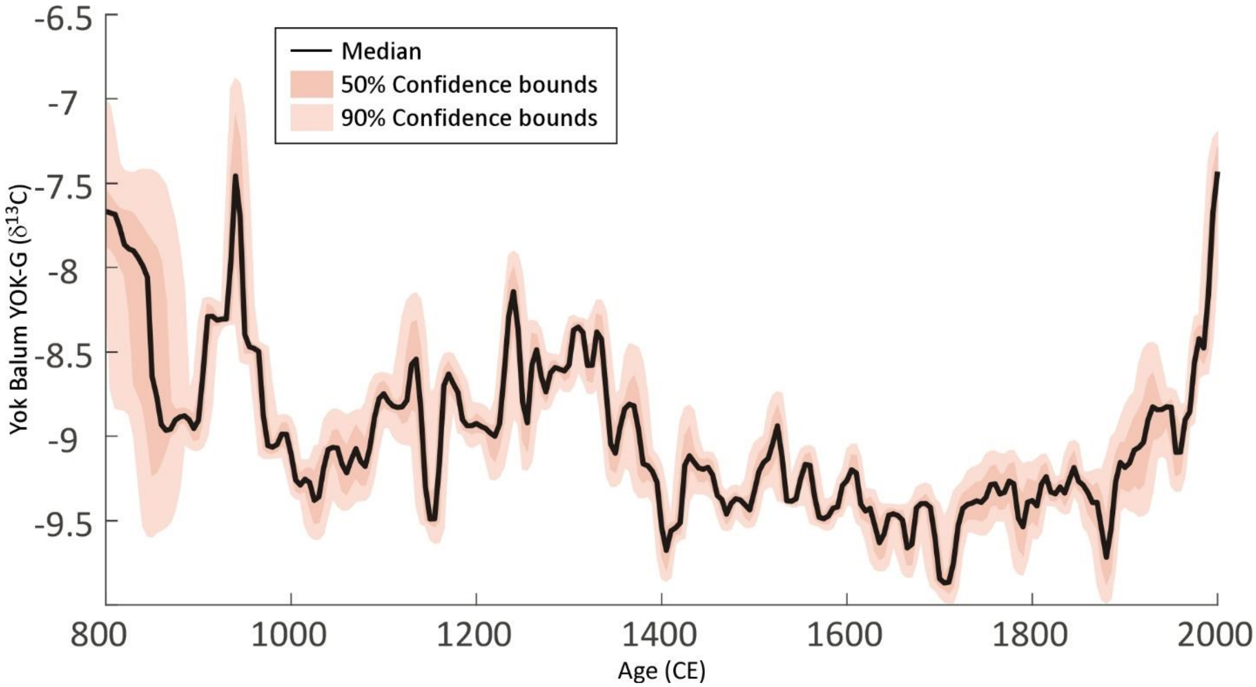

Figure S26. Median, 50% and 90% confidence bounds for the Yok Balum YOK-G speleothem δ^{13}C record (Asmerom et al., 2020). The plot shows the range of proxy values for 1000 age-depth models (same set of models used for the correlation analysis shown in Figure 5). Note that the graph shows the unconditional probability at each time step. That is, the graph does not represent correlations between time steps.

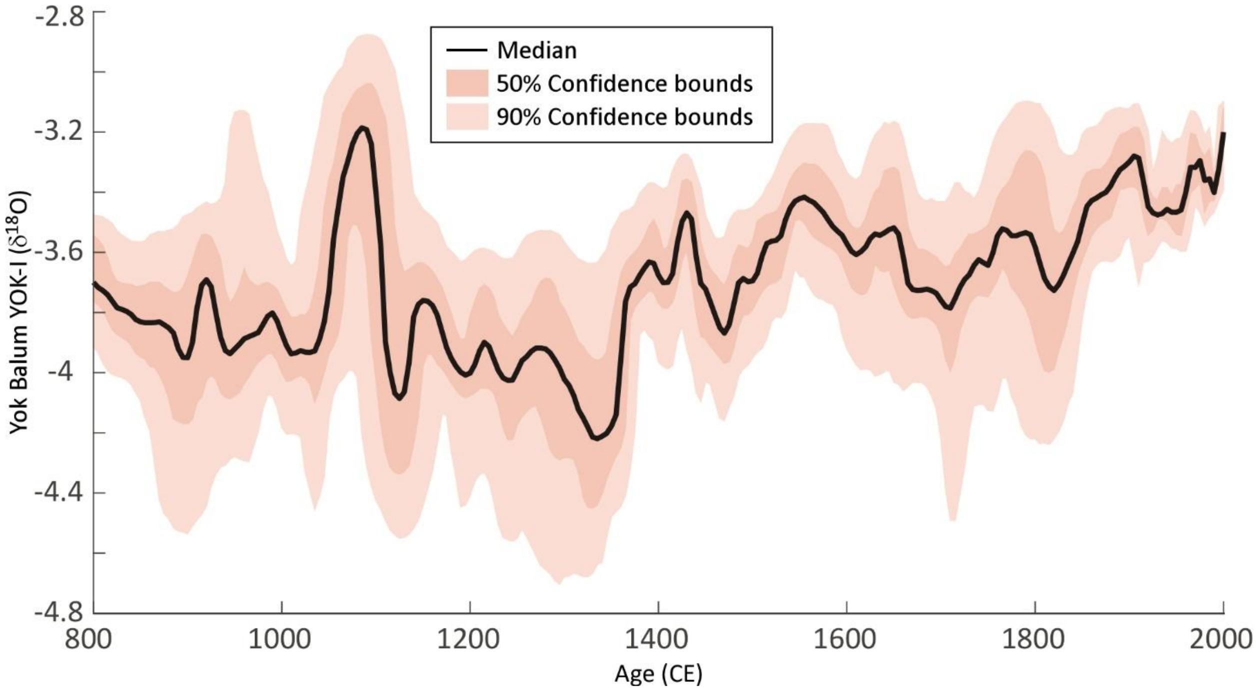

Figure S27. Median, 50% and 90% confidence bounds for the Yok Balum YOK-I speleothem $\delta^{18}O$ record (Kennett et al., 2012). The plot shows the range of proxy values for 1000 age-depth models (same set of models used for the correlation analysis shown in Figure 5). Note that the graph shows the unconditional probability at each time step. That is, the graph does not represent correlations between time steps.

References

Asmerom, Y., Baldini, J. U. L., Prufer, K. M., Polyak, V. J., Ridley, H. E., Aquino, V. V., et al. (2020). Intertropical convergence zone variability in the Neotropics during the Common Era. *Science Advances, 6*(7), eaax3644. https://doi.org/10.1126/sciadv.aax3644

Blaauw, M., & Christen, J. A. (2011). Flexible paleoclimate age-depth models using an autoregressive gamma process. *Bayesian Anal., 6*(3), 457-474. https://projecteuclid.org:443/euclid.ba/1339616472

Curtis, J. H., Hodell, D. A., & Brenner, M. (1996). Climate variability on the Yucatan Peninsula (Mexico) during he past 3500 years, and implications for Maya cultural evolution. *Quaternary Research, 46*(1), 37-47. https://doi.org/10.1006/qres.1996.0042

Harris, I., Jones, P. D., Osborn, T. J., & Lister, D. H. (2014). Updated high-resolution grids of monthly climatic observations – the CRU TS3.10 Dataset. *International Journal of Climatology, 34*(3), 623-642. https://doi.org/10.1002/joc.3711

Haug, G. H., Hughen, K. A., Sigman, D. M., Peterson, L. C., & Röhl, U. (2001). Southward migration of the Intertropical Convergence Zone through the Holocene. *Science, 293*(5533), 1304. https://doi.org/10.1126/science.1059725

Hernández, E., Obrist-Farner, J., Brenner, M., Kenney, W. F., Curtis, J. H., & Duarte, E. (2020). Natural and anthropogenic sources of lead, zinc, and nickel in sediments of Lake Izabal,

Guatemala. *Journal of Environmental Sciences, 96*, 117-126. https://doi.org/10.1016/j.jes.2020.04.020
Hodell, D. A., Brenner, M., Curtis, J. H., Medina-González, R., Ildefonso-Chan Can, E., Albornaz-Pat, A., & Guilderson, T. P. (2005). Climate change on the Yucatan Peninsula during the Little Ice Age. *Quaternary Research, 63*(2), 109-121. https://doi.org/10.1016/j.yqres.2004.11.004
Kennett, D. J., Breitenbach, S. F. M., Aquino, V. V., Asmerom, Y., Awe, J., Baldini, J. U. L., et al. (2012). Development and disintegration of Maya political systems in response to climate change. *Science, 338*(6108), 788-791. https://doi.org/10.1126/science.1226299
Medina-Elizalde, M., Burns, S. J., Lea, D. W., Asmerom, Y., von Gunten, L., Polyak, V., et al. (2010). High resolution stalagmite climate record from the Yucatán Peninsula spanning the Maya terminal classic period. *Earth and Planetary Science Letters, 298*(1), 255-262. https://doi.org/10.1016/j.epsl.2010.08.016
Obrist-Farner, J., & Rice, P. M. (2019). Nixtun-Ch'ich' and its environmental impact: Sedimentological and archaeological correlates in a core from Lake Petén Itzá in the southern Maya lowlands, Guatemala. *Journal of Archaeological Science: Reports, 26*, 101868. https://doi.org/10.1016/j.jasrep.2019.05.033
Reimer, P. J., Austin, W. E. N., Bard, E., Bayliss, A., Blackwell, P. G., Bronk Ramsey, C., et al. (2020). The IntCal20 Northern Hemisphere radiocarbon age calibration curve (0–55 cal kBP). *Radiocarbon, 62*(4), 725-757. https://doi.org/10.1017/RDC.2020.41
Schneider, U., Becker, A., Finger, P., Meyer-Christoffer, A., Rudolf, B., & Ziese, M. (2011). *GPCC full data reanalysis version 6.0 at 0.5◦: monthly land-surface precipita-tion from rain-gauges built on GTS-based and historic data*. Retrieved from: https://doi.org/10.5676/dwd_gpcc/fd_m_v6_050
Stansell, N. D., Steinman, B. A., Abbott, M. B., Rubinov, M., & Roman-Lacayo, M. (2013). Lacustrine stable isotope record of precipitation changes in Nicaragua during the Little Ice Age and Medieval Climate Anomaly. *Geology, 41*(2), 151-154. https://doi.org/10.1130/G33736.1
Stansell, N. D., Steinman, B. A., Lachniet, M. S., Feller, J., Harvey, W., Fernandez, A., et al. (2020). A lake sediment stable isotope record of late-middle to late Holocene hydroclimate variability in the western Guatemala highlands. *Earth and Planetary Science Letters, 542*, 116327. https://doi.org/10.1016/j.epsl.2020.116327
Willmott, C. J., & Matsuura, K. (2001). *Terrestrial Air Temperature and Precipitation: Monthly and Annual Time Series (1950–1999), Version 5.0.1. Center for Climatic Research*. Retrieved from: http://climate.geog.udel.edu/~climate/html_pages/README.ghcn_ts2.html
Winter, A., Zanchettin, D., Lachniet, M., Vieten, R., Pausata, F. S. R., Ljungqvist, F. C., et al. (2020). Initiation of a stable convective hydroclimatic regime in Central America circa 9000 years BP. *Nature Communications, 11*(1), 716. https://doi.org/10.1038/s41467-020-14490-y